Studies of the chemistry and physics of starless and prestellar cores

Olli Sipilä

ACADEMIC DISSERTATION

Department of Physics
Faculty of Science
University of Helsinki
Helsinki, Finland

Abstract

Concentrations of dense and cold gas embedded in gigantic molecular clouds, the so-called starless or prestellar cores, represent the initial stages of star formation in the interstellar medium. The dominating gas component in the cores is molecular hydrogen, but a variety of other elements such as helium, oxygen, carbon and nitrogen are also present in appreciable amounts. A notable addition to this list is deuterium which can, at the low temperatures prevalent in the cores, be treated as another element. In fact, it turns out that deuterium is increasingly important toward the very centers of the cores where the density is highest.

In addition to the gas, interstellar dust is also present in the cores with a total mass of about one hundreth of the total gas mass. Chemical interaction between the gas and the dust and the relatively high gas density allow for rich chemical evolution to take place during the lifetime of a core. The chemistry affects the gas temperature because the gas cools mainly by molecular line radiation, and the gas temperature in turn determines the thermal pressure which is mainly responsible for stabilizing the core against gravitational collapse. Consequently, the chemical composition of a core influences its physical evolution.

Observing the molecular line radiation emitted by the various chemical species yields information on, e.g., the kinematics and the temperature of the gas. We can also deduce molecular column densities based on observations. However, the observationally measured column densities are averages over different lines of sight and hence possible spatial variations in the number densities of the various species, and consequently in the gas temperature, can be difficult to detect. This is particularly important toward the centers of the cores where molecules are expected to freeze onto the surfaces of dust grains and hence to disappear from the gas phase. For this reason, numerical models of the chemistry are needed to correctly interpret the various observations. Indeed, studying the chemical and physical properties of starless and prestellar cores theoretically, using numerical methods, is the focus of this thesis which consists of five original journal articles.

In two of the articles, we discuss the chemistry of light deuterated ions in the context of the so-called complete depletion model, in which all elements heavier than helium are frozen onto the surfaces of dust grains. In the latter of these two articles, we expand upon the complete depletion model by explicitly taking into account the chemical evolution of heavier species preceding freeze-out, and our analysis yields the first theoretical prediction of the eventual depletion of the singly-deuterated hydrogen molecule, HD.

One of the articles focuses solely on the physics of starless and prestellar cores by studying their stability against gravitational collapse. For the physical core model

we choose the modified Bonnor-Ebert sphere, and in this article we present for the first time a stability condition for such a sphere. We find that the stability of the modified Bonnor-Ebert sphere is similar to that of the classical isothermal Bonnor-Ebert sphere.

One of the articles studies the interaction between the chemistry and physics in starless and prestellar cores. We combine chemical and radiative transfer modeling to derive estimates of the gas temperature based on simulated molecular abundances. We find that the gas temperature is expected to change by a 1-2 K during a typical core lifetime and conclude that this may have implications on the stability of the cores. Also, we find that the NH_3/N_2H^+ abundance ratio increases at very high densities, seemingly contradicting observations.

In one article, we study the chemical and physical properties of the starless core SL42. We fit observed $C^{18}O$ and N_2H^+ line profiles using simulated chemical abundances based on time-dependent and steady-state chemical models, and we find that the observed $C^{18}O$ abundance profile is well fitted by the steady-state model.

Acknowledgements

The work for this thesis began at the Observatory of the University of Helsinki and was completed at the Department of Physics after the two departments merged in 2010.

During the thesis work, I have greatly benefited from the advice of two supervisors. My primary supervisor, Docent Jorma Harju, has taught me a great deal not only about astrochemistry but also about astronomy in general. His advice – and patience – over the years has been invaluable to me, especially during the early stages of the thesis work when I knew next to nothing about astronomy, having graduated in theoretical physics. My second supervisor, Docent Mika Juvela, has been equally helpful in answering any of my questions concerning interstellar matter. His great expertise in numerical methods has made it possible for me to include all of the topics presented in this thesis. I would also like to express special thanks to Professor Emeritus Kalevi Mattila, who forwarded me to Mika Juvela when I asked after possible Ph.D. positions back in 2008, and thus effectively started my career as an astronomer.

I am indebted to the two pre-examiners, Professor Peter Schilke (Universität zu Köln, Germany) and Doctor Wolf Geppert (Stockholm University, Sweden) for a critical reading of this thesis. I would also like to express my thanks to Professor Tom Millar (Queen's University Belfast, Northern Ireland) for agreeing to act as the Opponent, and to Professor Karri Muinonen for acting as the Custos.

The thesis has been supported financially by the Academy of Finland, and also by the Väisälä Foundation of the Finnish Academy of Science and Letters.

During the thesis work, I have had the privilege to interact with extremely friendly people at the University of Helsinki. Being able to discuss matters not relating to work, especially at lunchtime, has contributed greatly to my sanity during the times when the thesis work felt less appealing, and for this I thank you all. I do not wish to produce a complete list of names here; you know who you are. I would also like to thank my family – my parents, my brother and his girlfriend – for their outstanding support over the years.

Finally, I want to express my most heartfelt thanks to my wife Tanja. It is difficult to express in words how much your constant support in both good and bad times, in sickness and in health, means to me. I love you.

Olli Sipilä
Helsinki, October 2013

List of publications

Paper I: O. Sipilä, E. Hugo, J. Harju, O. Asvany, M. Juvela, and S. Schlemmer, 2010, "Modelling line emission of deuterated H_3^+ from prestellar cores", Astronomy & Astrophysics, 509, A98

Paper II: O. Sipilä, 2012, "Radial molecular abundances and gas cooling in starless cores", Astronomy & Astrophysics, 543, A38

Paper III: O. Sipilä, P. Caselli, and J. Harju, 2013, "HD depletion in starless cores", Astronomy & Astrophysics, 554, A92

Paper IV: O. Sipilä, J. Harju, and M. Juvela, 2011, "On the stability of non-isothermal Bonnor-Ebert spheres", Astronomy & Astrophysics, 535, A49

Paper V: E. Hardegree-Ullman, J. Harju, M. Juvela, **O. Sipilä**, D.C.B. Whittet, and S. Hotzel, 2013, "Chemical and physical conditions in molecular cloud core DC 000.4–19.5 (SL42) in Corona Australis", The Astrophysical Journal, 763, 45

The articles are reprinted with permissions from *Astronomy & Astrophysics* and the AAS.

Contents

Chapter 1

Introduction

1.1 Starless and prestellar cores

Low-mass star formation starts with the gravitational contraction of condensations of dense and cold gas residing inside large molecular clouds. These condensations are called either *starless* or *prestellar* cores, and distinction between these two classes is made based on dynamical status. Starless cores are objects whose fate is unknown to us; such objects may either collapse, thus possibly initiating star formation, or they may eventually disperse due to "excess" internal pressure. Prestellar cores on the other hand show signs of initial stages of star formation, such as infall, and so these objects are identified as more or less definite precursors to stars. However, collapsing motions are difficult to detect owing to the very low infall speeds in the beginning of the collapse, so that it is difficult to determine the dynamical state of the core accurately through observations. In the chemistry models discussed in this thesis, we assume that the core is stable or its dynamical evolution is slow compared with the timescale of the chemistry. For the sake of conciseness, both starless and prestellar cores are here referred to together as "dense cores".

Dense cores have typical gas densities of $\gtrsim 10^4\,\mathrm{cm}^{-3}$ and temperatures of $\sim 10\,\mathrm{K}$ (di Francesco et al. 2007). The gas consists mainly of hydrogen (which is in molecular form owing to the high density), but other elements such as helium, oxygen, carbon and nitrogen are also present with fractional abundances (i.e., density divided by that of hydrogen) of $\sim 9\times10^{-2}$, $\sim 2.56\times10^{-4}$, $\sim 1.2\times10^{-4}$ and $\sim 7.6\times10^{-5}$, respectively (Wakelam & Herbst 2008, and the references therein). Also, trace amounts ($\lesssim 10^{-5}$) of heavier elements such as sulphur, silicon and iron are present. In addition to the gas, another major constituent of dense cores is *interstellar dust*, i.e., small solid particles with sizes of about 0.001 to 0.1 μm (Williams & Herbst 2002); the total mass of dust is about one hundreth of the total gas mass (Dyson & Williams 1997). The grains may consist of, e.g., carbonaceous material (e.g. Duley 1985; Witt & Schild 1988) or silicates (e.g. Draine & Li 2001; Li & Draine 2002). The smallest grains may even be polyaromatic hydrocarbons (e.g. d'Hendecourt et al. 1986).

Despite the low temperature and (in terrestrial terms) low density, the cores exhibit rich chemistry. In the gas phase, chemical evolution is initiated by cosmic ray ionization and followed by ion-molecule chemistry (see Chapter 2 for details and, e.g., van Dishoeck & Blake 1998 for a review). The gas and dust interact chemically: the various chemical species in the gas can collide with and stick onto the surfaces of dust
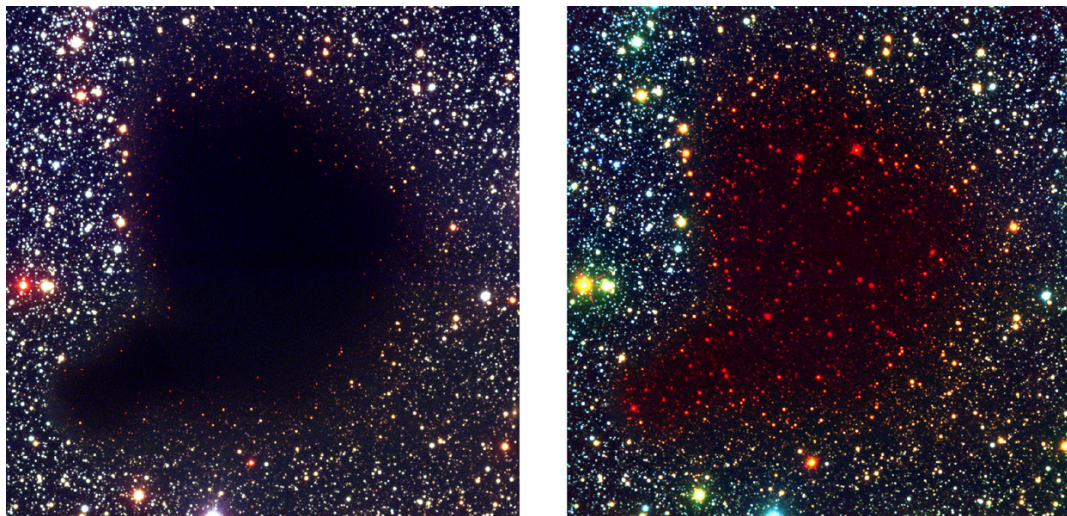
Figure 1.1: The dark cloud Barnard 68. On the left, the cloud is seen in the B, V, and I bands with wavelengths $0.44\,\mu$m, $0.55\,\mu$m and $0.90\,\mu$m, respectively. On the right, the B, I, and K $(2.2\,\mu$m) bands are shown. The B, V, and I band images have been taken with ESO's Very Large Telescope, while the K band image has been taken with ESO's New Technology Telescope. Image credit: ESO PR Photo 02c/01.

grains where they can react with each other and form more complex species. These species can then be returned to the gas phase via desorption. For example the formation of complex organic molecules in dense cores is attributed mainly to reactions on grain surfaces (see, e.g., the review by Herbst & van Dishoeck 2009).

The gas cools by molecular line radiation, and the strength of this process depends on the abundances of the various species (this issue is discussed in Chapter 2). Thus, chemical evolution affects the gas temperature and hence the internal pressure balancing the core against gravitational collapse. Consequently, studying chemical evolution in dense cores helps us to understand the initial stages of the star formation process.

1.2   Modeling dense cores

Molecular line radiation and continuum emission from the interstellar dust (to name two examples) allow us to directly study dense cores using observational methods. However, in order to analyze and understand the data gathered from observations, it is often necessary to develop theoretical models of the observed objects.

A famous example of theoretical modeling of a dense cloud is the study by Alves et al. (2001) of Barnard 68 (B68), a molecular cloud towards the southern constellation Ophiuchus. The cloud is depicted in Fig. 1.1, as observed in the B, V, and I bands on the left and in the B, I, and K bands on the right. The images exemplify one effect induced by the presence of dust grains, *dust extinction*, which occurs because dust grains efficiently scatter and absorb radiation at short wavelengths. Thus for example radiation in the visual band is, in effect, unable to penetrate the cloud. Infrared radiation however suffers less extinction and this is why the background stars are visible in the K band, and appear red in the picture. Alves et al. (2001)

derived the density structure of B68 by mapping the dust extinction, and found that the density profile is well fitted by a Bonnor-Ebert sphere (see Chapter 7). Using previous estimates of the distance of the cloud (125 pc; de Geus et al. 1989) and the temperature (16 K; Bourke et al. 1995), they derived estimates for various physical attributes of the core and found that the core should be unstable against gravitational contraction. Subsequently, the structure of B68 has been studied in more detail using line emission observations and chemical models (e.g. Bergin et al. 2002, 2006; Maret et al. 2007; Nielbock et al. 2012). These models constrain not only the abundances of the various chemical species in the cloud but also the physical structure – although Alves et al. (2001) assumed that the cloud is isothermal when deriving the density structure, subsequent modeling suggests that this may not be the case (and also that the dust and gas temperatures are not equal; Bergin et al. 2006).

Of course, B68 is not the only dense object that has been subject to modeling: chemical and/or dynamical models have been applied to study the properties of many prestellar cores such as L1544 (Caselli et al. 2002; Aikawa et al. 2005; Doty et al. 2005) and L183 (Dickens et al. 2000; Pagani et al. 2007), to name two examples.

To sum up the above, modeling observed dense cores helps us to understand their dynamical and chemical status, and through this to improve our understanding of the initial stages of (low-mass) star formation. Although we have applied our models to studying the properties of specific objects (Papers I and V), the main goal of this thesis is to study the chemical and physical properties of dense cores in general, through numerical methods.

1.3   The structure of the thesis

The thesis consists of an introductory review part discussing the main themes of the work, followed by five original journal articles. The articles have been published in the international peer-review journals Astronomy & Astrophysics (Papers I to IV) and The Astrophysical Journal (Paper V).

The introductory part is organized as follows. In Chapter 2, the various physical and chemical processes taking place in dense cores are discussed, with an emphasis on chemistry. Chapters 3 and 4 delve further into the specifics of core chemistry, discussing deuterium and spin states, respectively. Chapter 5 details the chemical model program developed during the thesis. In Chapter 6, simulated observations of line emission toward dense cores are discussed. Chapter 7 deals with the stability of the core model used in the thesis. In Chapter 8, the publications included in the thesis are summarized, and in Chapter 9, concluding remarks are given.

Chapter 2

The physics and chemistry of dense cores

In this thesis, we have studied chemical and physical processes taking place in starless and prestellar cores. This chapter gives an overview of these processes, and of their connections to each other.

2.1 Physical characteristics of dense cores

Dense cores are condensations of dense and cold gas – typically, the density of these objects is $n_{\mathrm{H}} \sim 10^4 \, \mathrm{cm^{-3}}$ (expressed in terms of the total number density of hydrogen nuclei) and the kinetic temperature is ~ 10 K. These are average values; in general, the cores present density and temperature structure. The density may vary by orders of magnitude across the core (decreasing toward the core edge), while the variation in temperature can be several K (Galli et al. 2002; Keto & Field 2005; Keto & Caselli 2010; Juvela & Ysard 2011; Paper II).

As noted in the Introduction, typically about 99% of the core mass is in the gas; the rest of the mass is made up of dust grains. At low density ($n_{\mathrm{H}} < 10^5 \, \mathrm{cm^{-3}}$), the gas and dust are generally at different temperatures. This is because they are heated and cooled by different processes and the thermal coupling between gas and dust is weak at low density. The main heating mechanism for grains is interstellar far-ultraviolet (FUV) radiation, which becomes increasingly attenuated toward the center of a core because of extinction. On the other hand, grains cool through emitting infrared (IR) radiation which penetrates the core relatively easily, so that the cooling efficiency is similar irrespective of the location of the grain in the core. These processes result in an inward-decreasing temperature profile for dust grains (e.g. Fig. 1 in Juvela & Ysard 2011). Unlike the dust, the gas is heated mainly by cosmic rays and cools by molecular line radiation. The cooling is increasingly inefficient toward the core center because of increasing optical depth, which causes an increasing tendency in the gas temperature toward the core center.

At high density ($n_{\mathrm{H}} > 10^5 \, \mathrm{cm^{-3}}$), however, the gas and dust are efficiently coupled through collisions. Because heat transfer is efficient only from the gas to the dust and not vice versa, the effect of the coupling is to significantly reduce the gas temperature as opposed to a situation where dust grains are not present, while leaving the dust temperature almost unchanged (Goldsmith 2001). As a result, $T_{\mathrm{gas}} \approx T_{\mathrm{dust}}$ at high
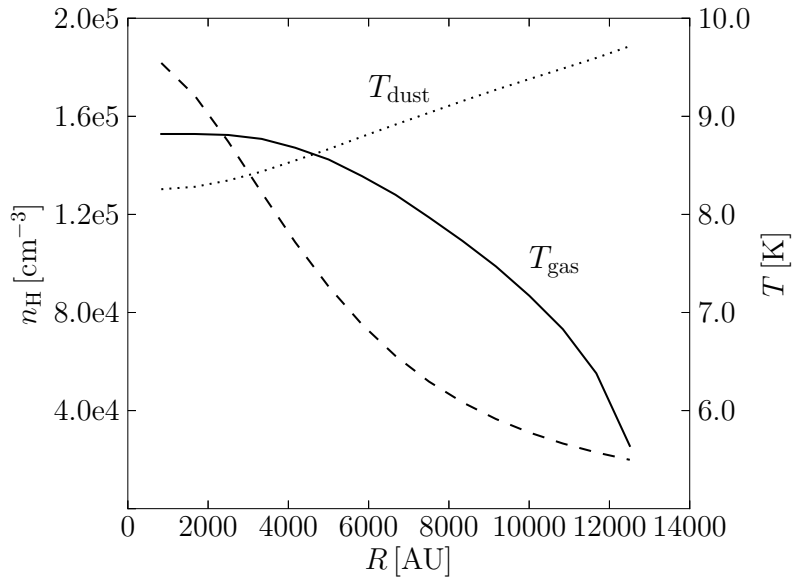
Figure 2.1: The gas (solid line) and dust (dotted line) temperatures as a function of core radius in a $1\,M_\odot$ modified Bonnor-Ebert sphere. Also plotted is the core density profile (dashed line). Adapted from Fig. 2 in Paper II.

density. The density-dependence of the two temperatures is demonstrated in Fig. 2.1, which is adapted from Paper II. The core model used here is a modified Bonnor-Ebert sphere (Ebert 1955; Bonnor 1956; Evans et al. 2001, Keto & Field 2005; Paper II), i.e., a gas sphere in hydrostatic equilibrium bounded by external pressure (see also Sect. 7.1). The core mass is $1.0\,M_\odot$. Evidently, the gas temperature differs clearly from the dust temperature at the core edge where density is low, but the two temperatures become coupled toward the dense center of the core. It should be noted that this model represents a deeply embedded core as it assumes visual extinction of $A_V = 10$ mag due to an external medium, and thus heating by the interstellar radiation field (ISRF) is minimal. For low values of A_V, the gas temperature is expected to rise as heating by the ISRF through the photoelectric effect becomes important (e.g. Keto & Caselli 2010; Juvela & Ysard 2011).

Along with the rest of the interstellar medium, the cores are subject to ionization: for visual extinction of $A_V \lesssim 4$ mag, the main source of ionization is UV photoionization whereas at higher values of A_V, ionization by cosmic rays becomes dominant (McKee 1989). (In this thesis, we only consider deeply embedded cores with a high external visual extinction of $A_V = 10$ mag, so that photoionization is negligible.) Ionization directly affects the chemistry (see Sect. 2.2), but it can also affect the stability of a core against gravitational collapse by enabling magnetic support as the ions freeze onto the magnetic field lines (this effect is, however, not considered in this thesis).

2.2 Chemical processes and gas-grain interaction

As mentioned in Sect. 2.1, dense cores consist of a gas and a dust component. During the course of core evolution, chemical reactions take place both in the gas phase and on the surfaces of dust grains. The two core components interact chemically

through adsorption (from the gas phase onto grain surfaces) and desorption (from grain surfaces to the gas phase). Below we discuss these processes in detail.

2.2.1 Gas-phase chemistry

There are many different types of chemical reactions occurring in the gas phase. Below, different reaction types are listed with emphasis on those types that are the most relevant for this thesis. However, before discussing different reaction types, let us first briefly review how the creation and/or destruction of a given chemical species in the various reactions can be studied numerically, as this is one of the main issues of the thesis. Consider a general chemical reaction

$$A + B \xrightarrow{k} C + D \,, \tag{2.1}$$

with an associated *rate coefficient* k (usually given in $cm^3 \, s^{-1}$), which is essentially a measure of the efficiency of the reaction. Generally, k is given in the form of a modified Arrhenius equation:

$$k = \alpha \left(\frac{T}{300 \, \text{K}} \right)^{\beta} e^{-\gamma/T} \,. \tag{2.2}$$

Here, β represents a possible temperature dependence of the reaction, while γ represents a possible activation energy. The above representation for k is valid for most gas-phase reactions, but some reaction types are parametrized differently. Below, when listing different reaction types, typical values for the α, β and γ coefficients and the functional form of k (if it differs from the above) are given so that the relative efficiencies of the reaction types can be assessed.

The information of consequence to astrochemical modeling is given by the *rate* with which a given species is created or destroyed. For example, in the above reaction the creation rate of species C is given by

$$\frac{dn(\text{C})}{dt} = k \, n(\text{A}) \, n(\text{B}) \,, \tag{2.3}$$

where $n(i)$ is the number density of species i (usually given in cm^{-3}); similarly, for example species A is destroyed with a rate $-k \, n(\text{A}) \, n(\text{B})$. The total rate of change in the number density of species X is thus given by

$$\frac{dn(\text{X})}{dt} = formation \ terms + destruction \ terms \,. \tag{2.4}$$

In this thesis, chemical evolution in dense cores is studied using this *rate equation method*. Rate equations can be applied in the gas phase because we can, in practice, always divide the object into volume elements large enough to contain all the reactants so that reactions can proceed. On the other hand, on the surfaces of individual grains the average number of particles of a given species may lie between 0 and 1, and stochastic methods are needed to accurately represent the reactions – we return to this issue in Sect. (2.2.3), where grain-surface chemistry is discussed in detail. Next, we proceed to introduce various reaction types in the gas phase. We also quote typical rate coefficients pertaining to each reaction type. It should be noted that only a minority of the numerical values quoted below are based on experimental work – in general, the rate coefficients are theoretical estimates.

Ion-neutral reactions

In dense cores, the gas-phase chemistry is driven mainly by ion-neutral reactions, because the electrostatic interaction between an ion and a neutral particle greatly increases the reaction cross-section compared to a similar neutral-neutral reaction. The importance of ion-neutral chemistry to the overall evolution of dense cores was recognized already in the 1970s (Herbst & Klemperer 1973; Oppenheimer & Dalgarno 1974). Indeed, even in modern astrochemical gas-phase reaction networks, the majority of reactions are ion-neutral reactions (e.g. Woodall et al. 2007).

As a first example of the importance of ion-neutral chemistry, consider the formation of the trihydrogen cation H_3^+ that is initiated when H_2 is ionized by a cosmic ray particle (crp):

$$H_2 + crp \longrightarrow H_2^+ + e^- + crp. \tag{2.5}$$
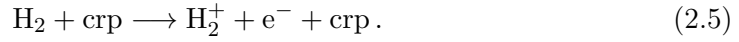
The H_2^+ thus formed then reacts with H_2 to produce H_3^+:

$$H_2^+ + H_2 \longrightarrow H_3^+ + H. \tag{2.6}$$

The trihydrogen cation H_3^+ is one of the most important ionic species for the chemistry of dense cores. This is because it is a precursor for multiple tracer species, such as HCO^+, N_2H^+, and H_2D^+, which are created in the respective ion-molecule reactions

$$H_3^+ + CO \quad \longrightarrow \quad HCO^+ + H_2 \tag{2.7}$$

$$H_3^+ + N_2 \quad \longrightarrow \quad N_2H^+ + H_2 \tag{2.8}$$

$$H_3^+ + HD \quad \longrightarrow \quad H_2D^+ + H_2. \tag{2.9}$$
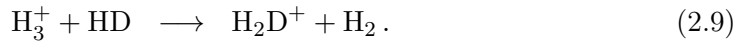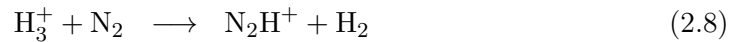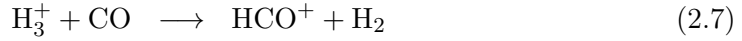
Reaction (2.9) is especially important for the development of deuterium chemistry in dense cores and is further discussed in Chapters 3 and 4.

In dense cores, the main coolant molecule is carbon monoxide, CO (Goldsmith 2001). It cannot be produced through atomic association, because the production path $C + O$ is radiative and hence extremely unlikely. Instead, CO can be produced for example through the following ion-molecule reaction pathway (including two ion-molecule reactions and a recombination reaction):

$$C^+ + OH \quad \longrightarrow \quad CO^+ + H \tag{2.10}$$

$$CO^+ + H_2 \quad \longrightarrow \quad HCO^+ + H \tag{2.11}$$

$$HCO^+ + e^- \quad \longrightarrow \quad CO + H. \tag{2.12}$$
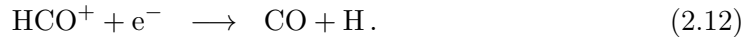
Ion-molecule reactions also play a part in the formation of ammonia, which is a useful probe of the kinetic temperature in dense cores (Ho & Townes 1983; Juvela et al. 2012). Ammonia formation begins with reactions of He^+ with nitrogen-containing molecules (such as N_2) that create N^+, which is then hydrogenated in abstraction reactions with H_2 until NH_4^+ is formed; NH_4^+ finally recombines with an electron, creating ammonia (see, e.g., Appendix A in Fontani et al. 2012).

The rate coefficient for ion-neutral reactions is given by (2.2); the typical α coefficient for an ion-neutral reaction is $10^{-9}\,\mathrm{cm^3\,s^{-1}}$ while, generally, $\beta = \gamma = 0$ so that the reactions are temperature-independent and barrierless (Duley & Williams 1984). Ion-neutral reactions are among the fastest reactions in the gas phase.

Neutral-neutral reactions

Almost all neutral-neutral reactions of relevance in dense cores are exchange reactions, such as

$$O + OH \longrightarrow O_2 + H \tag{2.13}$$

and

$$H + CH \longrightarrow C + H_2 \,; \tag{2.14}$$

as mentioned above in the case of CO formation, association reactions between neutral species are radiative and hence unlikely. Reaction (2.13) is actually the main gas-phase formation pathway of O_2 in dense cores. Many neutral-neutral reactions (k given by 2.2) have activation barriers (i.e. $\gamma \neq 0$; Duley & Williams 1984; Woodall et al. 2007) but those that do not, have typical α coefficients of $10^{-11} - 10^{-10}\,\mathrm{cm^3\,s^{-1}}$, making them less efficient than ion-neutral reactions.

Cosmic ray ionization and photoreactions induced by cosmic rays

The importance of cosmic ray (CR) ionization has already been exemplified above by reaction (2.5) when the formation mechanisms of H_3^+ and ammonia were discussed. As a further example, consider the gas-phase formation of water in dense cores. The process begins with the ion-molecule reaction

$$H_3^+ + O \longrightarrow OH^+ + H_2 \,. \tag{2.15}$$

OH^+ is subsequently hydrogenated in successive reactions with H_2 to H_3O^+, which recombines with an electron, creating either water or OH. This reaction chain demonstrates well the importance of CR ionization, as the water formation pathway depends on CR ionization both directly (through the formation of free electrons in CR ionization processes required for the recombination reactions) and indirectly (through the contribution of H_3^+).

The interiors of dense cores are usually well shielded from external UV radiation, but UV photons can be created inside the cores when H_2 molecules are ionized by secondary electrons created in CR ionization processes (Prasad & Tarafdar 1983; Gredel et al. 1989). These UV photons can then dissociate or ionize molecules.

The rate coefficient for cosmic ray ionization is given by $k_{\mathrm{CR}} = \alpha\zeta$, where a typical value for ζ is $1.3 \times 10^{-17}\,\mathrm{s^{-1}}$; the value of this parameter is however very uncertain and might vary greatly depending on the environment. Typical values for the α coefficient range from ~ 1 to $\sim 10^3$. We note that in the Ohio State University (OSU) chemical reaction set[1] utilized in this thesis, the rate coefficient for cosmic ray-induced photoreactions is given in the same form as for the CR ionization reactions, but other formulations also exist (see Woodall et al. 2007 for the rate coefficient utilized in the UMIST database).

Dissociative recombination

The various atomic/molecular ions taking part in ion-neutral chemistry can be destroyed in dissociative recombination (DR) reactions with electrons, which are

---

[1]See `http://www.physics.ohio-state.edu/~eric/`

created in dense cores primarily by the CR ionization of H_2 and He. An example of DR reactions is the dissociation of H_3O^+ already mentioned above. These reactions are very important for the evolution of dense cores, because they control the ionization degree which directly affects the ion-neutral chemistry and may also contribute to core stability by modifying the ambipolar diffusion timescale. The rate coefficient for DR reactions is given by (2.2); typically $\alpha \sim 10^{-7} - 10^{-6}\,\mathrm{cm^3\,s^{-1}}$ (OSU; Pagani et al. 2009), meaning that the reactions are very efficient. Notably, β is negative for DR reactions, so that the reactions are increasingly efficient at lower temperatures.

A special subset of dissociative gas-phase reactions worth a separate mention is gas-phase reactions involving grains. The importance of grains in controlling the gas-phase abundances of neutrals will be discussed below in the context of adsorption and desorption (and grain-surface reactions), but grains can also dissociate ions. In dense cores, most grains are negatively charged because of the efficiency of the radiative recombination reaction

$$\mathrm{g} + \mathrm{e}^- \longrightarrow \mathrm{g}^- + h\nu\,. \tag{2.16}$$

Neutral grains are most efficiently in created in neutralization reactions of atomic ions (such as $\mathrm{g}^- + \mathrm{C}^+ \to \mathrm{g} + \mathrm{C}$), but these reactions are not as efficient as reaction (2.16).

The α coefficients of DR reactions involving grains are similar to those of electron DR reactions (OSU; Walmsley et al. 2004; Flower et al. 2004). However, in the case that the grain and the incoming particle have different electric charges, electrostatic polarization can enhance the rate coefficient of the reaction by over an order of magnitude (Draine & Sutin 1987). When this is the case, a "J-factor" is added to (2.2) to account for polarization (Walmsley et al. 2004; Pagani et al. 2009; Paper I); the mathematical form of the J-factor is for negatively charged grains

$$\tilde{J}\,(Z = -1) = \left(1 + \frac{1}{\tau}\right)\left(1 + \sqrt{\frac{2}{2+\tau}}\right)\,, \tag{2.17}$$

and for neutral grains

$$\tilde{J}\,(Z = 0) = 1 + \sqrt{\frac{\pi}{2\tau}}\,, \tag{2.18}$$

where $\tau \equiv a_{\mathrm{g}} k_{\mathrm{B}} T_{\mathrm{gas}}/e^2$ is the "reduced temperature" (Draine & Sutin 1987). At core densities of $10^4 - 10^5\,\mathrm{cm^{-3}}$, the electron density is typically ~ 4 orders of magnitude higher than the grain density, so that electron DR reactions dominate over grain DR reactions. However, the density of grains increases with increasing core density (because the grain abundance is constant through the core, see Sect. 2.2.2) so that at the center of a dense core ($\sim 10^6\,\mathrm{cm^{-3}}$), grain DR recombinations become important owing to 1) the higher number density of grains, 2) increased reaction rates due to polarization and 3) the decrease of the fractional abundance of free electrons toward higher densities.

Other reaction types

The reaction types presented above are the most important to this thesis. However, there are additional types of reactions occurring in the gas phase – these are listed below, along with example reactions and typical rate coefficients (data

from OSU). Unless otherwise stated, the form of the rate coefficient for the following reaction types is given by (2.2).

Reactions between negative ions and neutral species: Various reactions (e.g. association, abstraction) involving anions and neutral species, such as the reaction $H^- + H_2O \longrightarrow OH^- + H_2$. Typically $\alpha \sim 10^{-9}\,cm^3\,s^{-1}$, and the reactions have no temperature dependence.

Radiative association: Associations of positive ions or neutrals with neutral species producing photons, such as the reaction $C^+ + H \longrightarrow CH^+ + h\nu$. Typically the reactions have strong negative temperature dependence and a low α coefficient $(\sim 10^{-17}\,cm^3\,s^{-1})$.

Electron ejection reactions: Association reactions of anions with neutrals ejecting an electron, such as in the reaction $H^- + N \to NH + e^-$; $\alpha \sim 10^{-10}\,cm^3\,s^{-1}$ with no temperature dependence. There is also one reaction between neutrals where an electron is ejected: $O + CH \longrightarrow HCO^+ + e^-$ with $\alpha = 2 \times 10^{-11}\,cm^3\,s^{-1}$ and $\beta = -0.44$.

Charge transfer reactions: Reactions where electric charge is transferred from one reactant to another, such as in the reaction $H^+ + Mg \longrightarrow Mg^+ + H$. Such reactions are reasonably fast, with typical $\alpha \sim 10^{-10} - 10^{-9}\,cm^3\,s^{-1}$.

Recombination reactions: There are three types of recombination reactions in the OSU data. In *radiative recombination* reactions, an electron incident on a positively charged species neutralizes the ion without dissociation, producing a photon. An example of such a reaction is $C^+ + e^- \longrightarrow C + h\nu$; the reactions are inversely dependent on temperature, with typical α values of $\sim 10^{-12}\,cm^3\,s^{-1}$.

In *cation-anion recombination* reactions, a cation and an anion neutralize each other, such as in the reaction $N^+ + H^- \to N + H$ (there are also a few neutralizing cation-anion abstraction reactions in the OSU data). For all of these reactions, $\alpha = 2.3 \times 10^{-7}\,cm^3\,s^{-1}$ and $\beta = -0.5$.

In *electron attachment* reactions (only four in the OSU data), an atom recombines with an electron to form an anion (e.g. $C + e^- \longrightarrow C^-$) – these are very inefficient reactions with $\alpha \sim 10^{-16} - 10^{-15}\,cm^3\,s^{-1}$.

Photoionization and photodissociation: These are reactions where an external photon ionizes or dissociates a neutral or an ion (e.g. $CH + h\nu \longrightarrow C + H$) – these processes should be distinguished from CR-induced photoionization/dissociation, which is an indirect process. The rate coefficient for photoreactions is given by

$$k_{\text{photo}} = \alpha\, e^{-\gamma A_V}\;; \tag{2.19}$$

typically $\alpha \sim 10^{-10}\,cm^3\,s^{-1}$ and $\gamma = 2 - 3$, so that these reactions are not significant in dense cores with appreciable shielding ($A_V \geq$ a few magnitudes).

2.2.2 Gas-grain interaction: adsorption and desorption

The presence of dust grains in dense cores affects not only the gas temperature and the extinction, but also the chemistry: gas-phase species can collide with and stick

onto the surfaces of grains in a process called *adsorption*. The "loss" of gas-phase species onto grain surfaces owing to adsorption is called *depletion* or *freeze-out*. The rate coefficient for adsorption of species i is given by

$$k_i^{\mathrm{ads}} = v_i\,\sigma\,S\,, \tag{2.20}$$

where $\sigma = \pi a_{\mathrm{g}}^2$ is the cross-section of the grain, $v_i = \sqrt{8k_{\mathrm{B}}T_{\mathrm{gas}}/\pi m_i}$ is the thermal speed of species i in the gas and S is a sticking coefficient, assumed in this thesis to be unity for all species[2]. In all of the papers included in this thesis, it is assumed that the grains are spherical which is of course a somewhat unrealistic assumption. However, the most important parameter for the grain chemistry in the present chemical model is the total grain surface area and not the shape of the grains, because we utilize the rate equation approach which is not sensitive to the grain morphology. The parameters controlling the grain surface area (see below) are here chosen in such a way that the total grain surface area agrees with observed values (see, e.g., Walmsley et al. 2004 for more discussion).

The rate of adsorption (in s^{-1}) of species i is given by

$$R_i^{\mathrm{ads}} = n_{\mathrm{g}} v_i\,\sigma\,S = \left(\frac{n_{\mathrm{g}}}{n_{\mathrm{H}}}\right) v_i\,\sigma\,S\,n_{\mathrm{H}}\,, \tag{2.21}$$

which yields the adsorption timescale as

$$t_i^{\mathrm{ads}} = \frac{1}{X_g\,v_i\,\sigma\,S\,n_{\mathrm{H}}}\,, \tag{2.22}$$

where n_{g} is the number density of grains and $X_{\mathrm{g}} \equiv n_{\mathrm{g}}/n_{\mathrm{H}}$ is their fractional abundance. For typical values[3] in dense cores ($T_{\mathrm{gas}} = 10\,\mathrm{K}$, $a_{\mathrm{g}} = 0.1\,\mu\mathrm{m}$, $n_{\mathrm{H}} = 10^5\,\mathrm{cm}^{-3}$, $X_{\mathrm{g}} = 2 \times 10^{-12}$), we recover $t^{\mathrm{ads}} \sim 10^5$ years (for $m_i \approx m_{\mathrm{H}}$), demonstrating that depletion can occur efficiently within a typical core lifetime (see Sect. 2.3). It should be noted that adsorption applies to neutral species only; it is conventionally assumed that ions do not stick onto grains but instead dissociate upon impact due to the energy associated with the interaction, returning neutral species into the gas phase (Flower et al. 2005).

While on the grain surface, an adsorbed species can react with other adsorbed species (see Sect. 2.2.3, where the binding of adsorbed species onto the surface is also discussed) or it can be returned back into the gas phase via thermal or non-thermal *desorption*. The rate coefficient for thermal desorption is given by (Hasegawa & Herbst 1993a)

$$k_i^{\mathrm{des,th}} = \nu_i\,e^{-E_i^{\mathrm{b}}/T_{\mathrm{dust}}} = \sqrt{\frac{2\,n_s\,k_{\mathrm{B}}\,E_i^{\mathrm{b}}}{\pi^2\,m_i}}\,e^{-E_i^{\mathrm{b}}/T_{\mathrm{dust}}}\,, \tag{2.23}$$

---

[2]It has been suggested that a lower sticking coefficient for nitrogen (and oxygen) could be responsible for the apparent resistance of nitrogen-containing species against depletion (Flower et al. 2006a), but the present consensus is that this may rather be due to the relatively low binding energies of N and N_2. Consequently, a sticking coefficient of unity is assumed in this thesis.

[3]The fractional abundance of grains can be calculated, in the case of spherical grains with a fixed radius and uniform density, as follows:

$$X_{\mathrm{g}} = \frac{n_{\mathrm{g}}}{n_{\mathrm{H}}} = dust-to-gas\ mass\ ratio \times \frac{mean\ mass\ of\ gas}{mass\ of\ a\ single\ grain} = R_{\mathrm{d}} \frac{\mu_{\mathrm{mol}}\,m_{\mathrm{H}}}{\frac{4}{3}\pi a_{\mathrm{g}}^3\,\rho_g}\,,$$

where $R_{\mathrm{d}} \sim 0.01$, $\rho_{\mathrm{g}} \sim 3.0\,\mathrm{g\,cm}^{-3}$ and μ_{mol}, the mean molecular weight, is ~ 1.4 (assuming hydrogen gas with $\sim 10\%$ He).

where ν_i is called the attempt frequency; n_s is the number density of adsorption sites on the grain ($\sim 10^{15}\,\text{cm}^{-2}$; Semenov et al. 2010; Taquet et al. 2012) and E_i^{b} is the binding energy of species i onto the grain surface. Note that the dimension of k^{des} is s^{-1}, so that the desorption timescale is simply the inverse of the rate coefficient.

In this thesis, non-thermal desorption is considered in the form of *cosmic ray desorption*, where a grain is heated to $T_{\text{dust}} \sim 70\,\text{K}$ upon a CR impact, allowing species on the surface to desorb (Hasegawa & Herbst 1993a; see also Léger et al. 1985). The rate coefficient for CR desorption is

$$k_i^{\text{des,CR}} = f(70\,\text{K})\,k_i^{\text{des,th}}(70\,\text{K})\,, \tag{2.24}$$

where the efficiency factor $f(70\,\text{K}) = 3.16 \times 10^{-19}$ for a CR ionization rate $\zeta = 1.3 \times 10^{-17}\,\text{s}^{-1}$ (Hasegawa & Herbst 1993a). We note that because of the very low temperature in dense cores, thermal desorption is negligible compared to CR desorption.

Because the CR desorption mechanism depends strongly on the binding energy of the species, it is instructive to compare the desorption timescales of two different species with different binding energies. Consider H and CO, with binding energies of $450\,\text{K}$ and $1150\,\text{K}$ (assuming a water ice surface; Garrod & Herbst 2006). The timescales for the CR desorption of these species can be then calculated from equations (2.23) and (2.24):

$$t_{\text{H}}^{\text{des,CR}} \sim 20\,\text{years};\ \ t_{\text{CO}}^{\text{des,CR}} \sim 1.6 \times 10^6\,\text{years}\,. \tag{2.25}$$

The difference between the desorption timescales of the two species is dramatic and demonstrates that weakly bound species (such as H) are not expected to be found in abundance on grain surfaces.

In addition to the above, other (non-thermal) desorption mechanisms have been considered in the literature. For example, it has been proposed that the energy released in exothermic reactions on grains can result in the desorption of surface species (Allen & Robinson 1975; Garrod et al. 2007; Roberts et al. 2007; Cazaux et al. 2010). This is implicitly assumed in Paper I, where the chemical model considers gas-phase chemistry only with the exception of H_2, HD, and D_2 formation on grains; the molecules are assumed to desorb immediately upon formation. Another possible desorption mechanism is photodesorption, whereby absorption of a UV photon may lead to desorption (recently: Garrod & Pauly 2011; Taquet et al. 2013). The latter mechanism has not yet been implemented into the chemical model developed in this thesis. It is unclear to what extent the inclusion of photodesorption would affect the results of this thesis. For example, the photodesorption of water on the grain surfaces does not in most cases lead to the desorption of OH (Taquet et al. 2013; see also Andersson & van Dishoeck 2008), which could be quickly rehydrogenated after the dissociation of H_2O. On the other hand, Keto & Caselli (2010) and Caselli et al. (2012) have argued that photodesorption processes may be needed to explain, e.g., the observed flux of CO isotopologs toward L1544. Finally, we note that Léger et al. (1985) have suggested that desorption due to X-rays may also be important for small grains.

2.2.3   Binding, diffusion and grain-surface reactions

Binding of chemical species onto grain surfaces

Chemical species adsorbed onto dust grains can be bound to the surface in a variety of ways. The weakest, but in dense cores the most common, binding mechanism is *physisorption*, which means that a Van der Waals (i.e. dipole-dipole) bond exists between the surface and the adsorbed species. In the case that the adsorbed species has enough energy and the surface is suitable, the adsorbed species can also form a covalent bond with the surface in a process called *chemisorption*. This process is however highly unlikely at $10\,\mathrm{K}$ since the barrier against chemisorption can be as high as $\sim 10000\,\mathrm{K}$ (Cazaux & Spaans 2009) – for comparison, typical binding energies associated with physisorption (on a water ice surface; see below) are of the order of $1000\,\mathrm{K}$ (Garrod & Herbst 2006).

Recently, the effect of porosity as a trapping mechanism has been investigated (Perets & Biham 2006; Taquet et al. 2012). Pores are essentially holes in the surface where species can be trapped; increasing the porosity of a grain has the effect of increasing the time spent by, and thus also the abundance of, volatile species (such as H) on the grain surface and thus increasing the formation rate of stable species (Taquet et al. 2012).

Yet another method of efficiently trapping species on grain surfaces is to consider a two-layer model separating the ice into a chemically active surface layer and an unreactive mantle (Hasegawa & Herbst 1993b; Garrod & Pauly 2011; Taquet et al. 2012). Exchange of species between the mantle and the surface layer is allowed, but reactions (and adsorption/desorption) only occur in the surface layer. Inclusion of this mechanism into the surface reaction scheme decreases in particular the amount of radicals available for reactions because they are trapped in the mantle, which decreases the formation efficiencies of stable species (Taquet et al. 2012).

The binding energies of the various species on the grain depend on the properties of the surface (Cuppen & Herbst 2007). It is customary in astrochemical modeling to consider binding energies related to either a pure ice surface (i.e. assuming some initial ice abundance) consisting of, e.g., CO or H_2O (Bergin & Langer 1997; Flower et al. 2005; Garrod & Herbst 2006; Taquet et al. 2012) or to a bare grain (Allen & Robinson 1977; Aikawa et al. 1997, 2001; Cazaux et al. 2010). In the context of dense cores, neither approach is strictly realistic because grains accumulate ice mantles over time and the relative abundances of the various ice constituents change with time. Some models have accounted for this (e.g. Cuppen & Herbst 2007; Garrod & Pauly 2011), but it remains unclear whether considering dynamic binding energies has an appreciable effect in dense cores compared to models with constant binding energies. As an approximation, constant binding energies pertaining to a water ice surface are considered in this thesis.

Of the binding mechanisms introduced above, only physisorption is considered in this thesis, and possible inclusion of the other mechanisms into the model is left for future work.

Diffusion of species on the grain surface

Numerical models of grain-surface reactions are based on a view of the grain

surface as a lattice with distinct sites where chemical species can be bound; particles on the grain surface can move from one site to an adjacent site[4] by thermal hopping (or perhaps by quantum-mechanical tunneling, see below). The thermal diffusion rate of species i, i.e., the inverse of the timescale for the species to "scan" the surface of the grain, is given by (Hasegawa et al. 1992)

$$R_i^{\text{diff,th}} = \frac{\nu_i}{N_s} e^{-E_i^{\text{diff}}/T_{\text{dust}}} , \qquad (2.26)$$

where ν_i is the attempt frequency introduced in reaction (2.23), $N_s = 4\pi a_{\text{g}}^2 n_s$ is the number of binding sites on the grain (assuming again a spherical grain) and E^{diff} is the diffusion energy. The binding energy and diffusion energy are related through $E^{\text{diff}} = \varepsilon E^{\text{b}}$; the value of ε is a source of uncertainty in chemical models, typical assumed values ranging from 0.3 to 0.8 (Hasegawa et al. 1992; Ruffle & Herbst 2000; Cuppen et al. 2009; Taquet et al. 2012).

The possibility of quantum tunneling of light species as a diffusion mechanism has also been studied in the literature. However, it remains a matter of debate whether tunneling can actually occur on grain surfaces. The often-cited work of Katz et al. (1999) argues against tunneling, while some modeling (e.g. Cazaux & Tielens 2004) and experimental (e.g. Goumans & Andersson 2010) works support the idea of tunneling. In Papers II and III, the effect of including tunneling is studied; the rate of diffusion by tunneling is given, following Hasegawa et al. (1992), by

$$R_i^{\text{diff,q}} = \frac{\nu_i}{N_s} \exp[-2 \, (a/\hbar) \, (2 \, m_i \, k_{\text{B}} \, E_i^{\text{diff}})] , \qquad (2.27)$$

where a is the barrier width (assuming a rectangular barrier). We note that in addition to the above, alternative definitions for the tunneling timescale also exist (e.g. Le Petit et al. 2009).

Surface reactions

In the literature, two different mechanisms for grain-surface reactions are considered. In the *Langmuir-Hinshelwood* (LH) mechanism (Langmuir 1922; Hinshelwood 1940), two physisorbed species mobile on the grain surface can meet at a binding site, in which case a chemical reaction can occur. The rate coefficient of such a reaction is given in the case of purely thermal diffusion by

$$k_{ij} = \alpha \, \kappa_{ij} \, (R_i^{\text{diff,th}} + R_j^{\text{diff,th}}) \, / n_{\text{g}} \qquad (2.28)$$

(Hasegawa et al. 1992). Here, α represents a possible branching ratio, and κ_{ij} is the reaction probability. For exothermic reactions without activation energy, $\kappa_{ij} = 1$, but for endothermic reactions or exothermic reactions with activation energy, $\kappa_{ij} = \exp(-E_{\text{a}}/T_{\text{dust}})$ (Hasegawa et al. 1992). The reaction rate is then given by

$$R_{ij} = k_{ij} \, n(i_s) \, n(j_s) , \qquad (2.29)$$

where $n(X_{\text{s}})$ is the number density of species X on the grain surface.

---

[4]This applies if the species is physisorbed. Chemisorption, i.e., the formation of a covalent bond, traps the species in place.

If quantum tunneling is included, the mathematical form of the reaction probability κ_{ij} has to be modified. In Papers II and III, we have considered the formulation of Hasegawa et al. (1992; see also Tielens & Hagen 1982):

$$\kappa_{ij} = \exp[-2\,(a/\hbar)\,(2\,\mu\,k_{\mathrm{B}}\,E_{\mathrm{a}})]\,, \tag{2.30}$$

where μ is the reduced mass. If tunneling is included, $R^{\mathrm{diff,th}}$ should be replaced with $R^{\mathrm{diff,q}}$ in Eq. (2.28).

In the *Eley-Rideal* (ER) reaction mechanism, atoms and molecules incident on a grain land on top of an already adsorbed species, possibly resulting in a chemical reaction (alternatively, the indicent atom/molecule can just bounce back into the gas phase without reacting). The ER reaction mechanism should however be negligible at low temperatures compared to the LH mechanism (depending also on the grain material; Cazaux et al. 2008), and is not included in this thesis.

Surface reactions are very important for the overall evolution of the chemistry in dense cores. The largest impact is due to atomic hydrogen, which is able to scan the surface rapidly due to its low mass and low binding energy, and can thus usually react before being desorbed. This can be justified by using Eq. (2.26), from which we recover for the diffusion timescale of H as

$$t_{\mathrm{H}}^{\mathrm{diff,th}} = \left(R_{\mathrm{H}}^{\mathrm{diff,th}}\right)^{-1} \sim 16 \text{ years}\,, \tag{2.31}$$

assuming $\varepsilon = 0.77$ and otherwise same values as used in deriving (2.25). This shows that even though a single hydrogen atom may spend on average only tens of years on a grain, it is possible for a hydrogen atom to scan the entire surface of the grain before it is desorbed. Consequently, hydrogenation reactions are efficient on grain surfaces. One particularly important example of this is H_2 formation on grains (e.g. Gould & Salpeter 1963; Hollenbach & Salpeter 1971) – even though H_2 is the simplest possible molecule, it cannot (in dense core conditions) be produced efficiently in the gas phase because the $H + H$ association reaction is radiative, i.e., the H_2 molecule is produced in an excited state and the excess energy needs to be quickly radiated away before the molecule dissociates. Typically, the timescale for emitting a photon is much longer than the vibrational timescale, so that the H_2 molecules dissociate upon formation practically every time (see Duley & Williams 1984). The reaction can however occur efficiently on the surface of a grain, which can absorb the excess energy of the H_2^* complex and thus stabilize the molecule (i.e. the grain acts as a third body in the reaction). The H_2 molecules created in this way can then desorb, regenerating the gas phase H_2 abundance.

The surface reaction scheme discussed above is based on the rate equation approach that deals with the number densities of the various species, which are essentially average quantities. However, on the surfaces of very small grains where the average number of atoms/molecules of a given species may be smaller than unity, the rate equation method fails. Naturally, a reaction cannot occur if one of the reactants is not present, but the rate equation method assumes that reactions always occur if the abundances of both species are nonzero (even if either is < 1). Therefore, reactions on small grains, or in any situation where average abundances are smaller than unity, should be treated with a stochastic rather than a deterministic approach. To this end, alternative approaches (Monte Carlo, master equation etc.) to the description of grain surface chemistry have been developed (Charnley et al. 1997; Biham et al.

2001; Vasyunin et al. 2009). Modifications to the rate equation method have also been suggested (Caselli et al. 1998; Garrod 2008; Du & Parise 2011). In this thesis, however, we consider faily large grains ($a_\mathrm{g} = 0.1\,\mu\mathrm{m}$) so that rate equation method should be adequate (see, e.g., Garrod 2008) and hence alternative methods are not considered.

2.3 How chemistry affects the gas temperature

In dense cores, several species (such as C and H_2O) contribute to the cooling of the gas, but the largest effect is due to CO (Goldsmith & Langer 1978; Neufeld et al. 1995; Goldsmith 2001). However, because of the low density ($\sim 10^4$ cm^{-3}) and low temperature (~ 10 K) of these objects, chemical evolution proceeds fairly slowly – the time required to reach chemical steady-state can be longer than $\sim 10^7$ years if gas-grain interaction is taken into account (see, e.g., the results of Garrod et al. 2007). This timescale is longer than the expected lifetimes of molecular clouds (the highest timescales are of the order of $\sim 10^6 - 10^7$ years, depending on the collapse mechanism; Hartmann et al. 2001; Mouschovias et al. 2006). Owing to the generally slow chemical evolution and different adsorption/desorption timescales of the various species, it is prudent to ask whether the contributions of the various species to the core cooling change with time and to what extent this may affect the gas temperature. Time-evolution could be especially important for the cooling by CO as it depletes onto grain surfaces.

This issue is studied in Paper II (and in Paper III), where the chemical model developed during this thesis is combined with a radiative transfer model (Juvela 1997) to produce semi-self-consistent estimates of both the chemical abundances and the gas temperature (see also Chapter 5). The method naturally allows to study the problem also in the other direction, i.e., whether a change in gas temperature affects the chemistry. It is found that the gas temperature does change with time owing to depletion effects, but the change in T_gas may be only $\sim 1 - 2$ K during a typical core lifetime (in line with previous studies by Bergin et al. 2006 and Keto & Caselli 2008). However, a (small) change in T_gas affects chemical abundances only marginally, reflecting the weak temperature dependence of ion-molecule chemistry. Of course, while a $\sim 1 - 2$ K change in T_gas may seem small, even such a small change could have implications on the stability of a core; we return to this issue in Chapter 7.
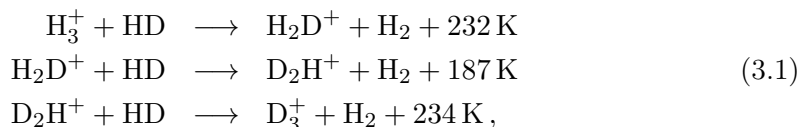
Chapter 3

Deuterium chemistry

Hydrogen (^{1}H, also called protium) has two isotopes, deuterium (^{2}H, or D) and tritium (^{3}H). While the latter is radioactive with a half-life of about 12.3 years, deuterium is stable and is found in appreciable abundance in the interstellar medium (ISM). Deuterium was originally created during the Big Bang nucleosynthesis, a time period of a few minutes until about twenty minutes after the beginning of the Universe. As no known efficient deuterium creation mechanisms are known in the present universe, practically all D found today is primordial. D and H have an equal amount of protons and thus one could expect them to behave chemically similarly, but their large mass ratio (2) leads to relatively large differences in zero-point vibrational energies in chemical compounds. This allows one to treat them as distinct species at low temperatures.

The present day abundance of D with respect to H in the Local Bubble is $\sim 1.6 \times 10^{-5}$ (Linsky 2003). Despite the fact that the amount of deuterium might vary somewhat depending on location in the Milky Way, this value is often used in chemical modeling (e.g. Walmsley et al. 2004; Taquet et al. 2013). The quoted value is about an order of magnitude lower than typical C and O abundances in the interstellar medium (Cardelli et al. 1993; Meyer et al. 1998). In dense cores, deuterium is not in atomic form but locked into HD, because HD is efficiently produced on grain surfaces already at low visual extinction (Cazaux et al. 2011). HD initiates deuterium chemistry in dense cores, as we will see below.

In this chapter, deuterium chemistry in dense cores is reviewed. We discuss the general features of deuterium chemistry, and its implementation into the chemical model developed during this thesis. The chapter concludes with a discussion of the impact of deuterium chemistry on the abundances of undeuterated species.

3.1 The progression of deuterium chemistry in dense cores

As noted above, deuterium is in dense cores locked into HD. Deuterium chemistry is initiated when HD reacts with H_3^+ in the following exothermic ion-neutral reactions

$$
\begin{aligned}
H_3^+ + HD &\longrightarrow H_2D^+ + H_2 + 232\,K \\
H_2D^+ + HD &\longrightarrow D_2H^+ + H_2 + 187\,K \\
D_2H^+ + HD &\longrightarrow D_3^+ + H_2 + 234\,K,
\end{aligned}
\tag{3.1}
$$

where the exothermicities of the reactions (Hugo et al. 2009) have been explicitly marked. We return to these reactions in Chapter 4. H_2D^+ and D_2H^+ are important probes of the central areas of dense cores (see Chapter 6) but in addition to this, the deuterated forms of H_3^+ play an important part in the continuation of deuterium chemistry after the initiation reactions presented above, because of their ability to donate deuterons to other species. For example, H_2D^+ readily reacts with abundant species such as CO and N_2 to produce other deuterated species:

$$H_2D^+ + CO \longrightarrow \left\{ \begin{array}{l} DCO^+ + H_2 \\ HCO^+ + HD \end{array} \right. \tag{3.2}$$

$$H_2D^+ + N_2 \longrightarrow \left\{ \begin{array}{l} N_2D^+ + H_2 \\ N_2H^+ + HD \end{array} \right. . \tag{3.3}$$
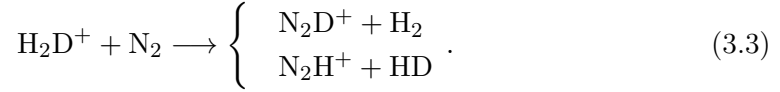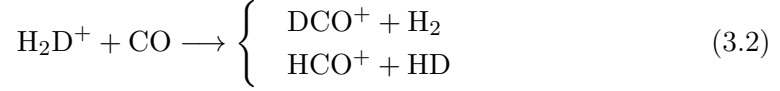
The branching ratios of the above reactions are not necessarily 1:1 – this issue is discussed below in Sect. 3.2.
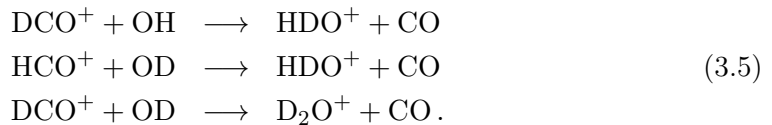
Reactions (3.1) to (3.3) are also important for the progression of deuterium chemistry on grain surfaces, because electron recombinations of the deuterated ions can produce atomic D, which can then be adsorbed onto grain surfaces. An example of such a recombination reaction is $D_3^+ + e^- \longrightarrow D + D + D$. Indeed, many deuterated species are efficiently formed on grains rather than in the gas phase. One example of this is HD which, just like its pure hydrogen counterpart H_2, cannot be efficiently produced in the gas phase but is instead produced on grains through H + D association. Another example is HDO, which is in dense cores produced through deuterated analogs of the $H + O \longrightarrow OH$ and $H + OH \longrightarrow H_2O$ reactions, and can become one of the main deuterium carriers on grain surfaces in physical conditions appropriate to the centers of dense cores (Aikawa et al. 2012; Taquet et al. 2013; Paper III).

3.2 Inclusion of deuterium chemistry in the chemical model

Most of the chemical reactions included in the chemical model used in this thesis originate in the OSU data that does not include deuterium. To study deuterium chemistry, we have (in Paper III) extended the OSU reaction network to include deuterated reactions by writing a routine to "clone" chemical reactions involving species with up to 4 atoms (see below) – cloning means in this case that in applicable reactions, deuterons are substituted in place of protons which in many cases produces multiple variants of the original reaction. For example, the reaction

$$HCO^+ + OH \longrightarrow H_2O^+ + CO, \tag{3.4}$$

when cloned, produces three new reactions

$$\begin{array}{rcl} DCO^+ + OH & \longrightarrow & HDO^+ + CO \\ HCO^+ + OD & \longrightarrow & HDO^+ + CO \\ DCO^+ + OD & \longrightarrow & D_2O^+ + CO . \end{array} \tag{3.5}$$

The rate coefficients of the above cloned reactions are assumed to be the same as for the original reaction. In principle, substituting a deuteron in place of a proton in a

reaction should affect the reaction rate coefficient because of the increased total mass of the reactants. This issue is however not straightforward and laboratory data is only available for a limited number of reactions. Therefore we have made the simplifying assumption that the rate coefficient is not altered in the cloning process (see also, e.g., Rodgers & Millar 1996; Albertsson et al. 2013).

However, in reactions where the position of the deuteron in the products is ambiguous, such as in the reaction

$$NH^+ + H_2O \xrightarrow{k} NH_2^+ + OH, \tag{3.6}$$

one needs to determine the branching ratios of the deuterated reactions. Reaction (3.6), when deuterated, results in 9 new reactions including for example the reactions

$$NH^+ + HDO \xrightarrow{\frac{2}{3}k} NHD^+ + OH$$

$$NH^+ + HDO \xrightarrow{\frac{1}{3}k} NH_2^+ + OD. \tag{3.7}$$
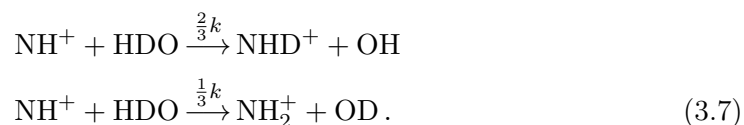
The above branching ratios result from a statistical approach to deuteration; we assume that the pool of (in this case) two protons and one deuteron is completely scrambled in the reaction. This should be a valid assumption as long as the intermediate complex exists long enough, and if the exothermicity of the reaction is much greater than the difference in the zero-point energies of the reactants and products. Our cloning process is similar to that presented in Rodgers & Millar (1996) and Albertsson et al. (2013). While this approach may not always be appropriate, using instead, e.g., 1:1 branching ratios for the above reactions should not make a large difference for the deuterium chemistry as a whole, as discussed by Rodgers & Millar (1996).

When deuterating reactions, one needs to take care that no unphysical reactions are created in the process. For example, in reactions where either H_3^+ or one of its deuterated forms donates a proton (or a deuteron), such as in the reaction between D_2H^+ and H_2O, the end result cannot be $HD_2O^+ + H_2$ – provided that the reaction indeed progresses through proton donation and not by oxygen abstraction. To avoid such errors, the deuteration routine is designed to analyze the type of the reaction being deuterated and decide on the possible products based on the reaction type.

From the above it is evident that the reaction cloning process introduces not only new reactions but also new species into the model. One thus needs to determine the binding energies of the deuterated species if gas-grain interaction is to be included in the model. In general, the binding energy of a given deuterated species is expected to be larger than that of the corresponding undeuterated species (Tielens 1983). However, because the absolute values of the binding energies are uncertain, we have assumed that the binding energy of a given deuterated species onto grain surfaces is equal to the binding energy of the corresponding undeuterated species. This approach has been followed also by, e.g., Cazaux et al. (2010) and Taquet et al. (2013).

The deuteration routine discussed above and in Paper III is designed to deuterate only those reactions that include species with a maximum of four atoms. The four-atom cutoff was chosen in order not to blow up the size of the reaction network[1] and

---

[1] A full deuteration of the OSU reaction set results in ~ 50000 reactions; see Albertsson et al. (2013).
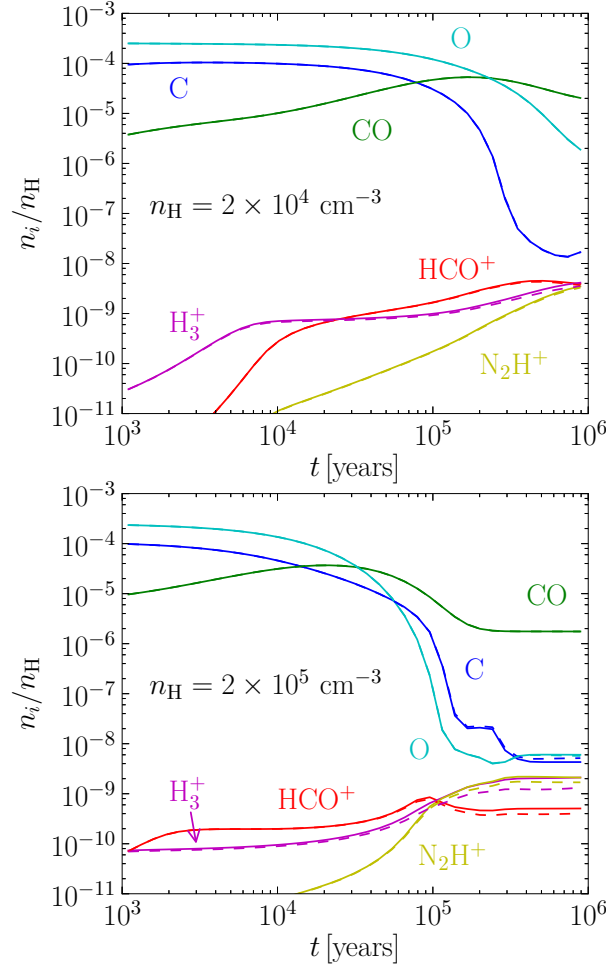
Figure 3.1: The abundances of selected species (indicated in the figure) as functions of time at two different densities. Solid lines represent a model where deuterium is excluded, while dashed lines represent a model with deuterium included.

thus greatly increase the time required for model calculations. Furthermore, Paper III focuses on the chemistry of light deuterated species and for this analysis the four-atom cutoff is sufficient. Extending the deuteration routine to handle more complex species would be relatively straightforward.

3.3   The impact of deuterium on the overall chemistry

The inclusion of deuterium into the gas-phase and grain-surface reaction sets more than doubles the total amount of reactions, even though only the species with up to four atoms are deuterated. A practical consequence of this is the introduction of many additional formation and destruction pathways for the undeuterated species. It is thus fair to ask whether the inclusion of deuterium into the model will significantly affect the abundances of undeuterated species; if this was the case, then comparison between models excluding D and those including D would be difficult, and this would

also affect the interpretation of observations.

To illustrate this issue, Fig. 3.1 presents the results of model calculations at two different densities studying the effect of including deuterium on the abundances of non-deuterated gas-phase species at $T_{\mathrm{gas}} = T_{\mathrm{dust}} = 10\,\mathrm{K}$. Evidently, the inclusion of deuterium into the model has, in general, little effect on the abundances of the various species. However, the abundances of ions in particular are slightly affected at late times, more strongly with increasing density. This can be explained as follows. In an undepleted environment, H_3^+ reacts preferentially with abundant neutral species such as CO and N_2 instead of HD – therefore, the deuteration of H_3^+, and hence the creation of H_2D^+, is suppressed until the neutrals start to deplete onto grain surfaces. At $n_H \sim 10^4\,\mathrm{cm}^{-3}$, the depletion timescale is $\sim 10^6$ years and consequently reactions such as (3.2) and (3.3) cannot proceed efficiently even in a timescale of 10^6 years. At $n_H \sim 10^5\,\mathrm{cm}^{-3}$, depletion is more efficient (with a timescale of about 10^5 years) and ions are partly deuterated, which slightly decreases the abundances of the undeuterated counterparts.

As suggested by Fig. 3.1, the division of the various species into their deuterated and undeuterated forms and the associated increase of the H/D ratio of a given species above the interstellar H/D ratio of $\sim 1.6 \times 10^{-5}$, the *deuterium fractionation*, is minimal at low/intermediate density but becomes more important at higher densities. To further demonstrate the efficiency of deuterium fractionation at high density, Fig. 3.2 shows the abundance ratios of the deuterated and undeuterated forms of selected species as functions of time at two different densities. Evidently, deuterium fractionation increases with density; at $n_H \sim 10^6\,\mathrm{cm}^{-3}$, the deuterated/undeuterated abundance ratio of a given species can be as high as ~ 1.

The figure displays three distinct important issues related to deuterium chemistry in dense cores. 1) Deuterium chemistry is highly time-dependent. 2) The degree of deuterium fractionation is not (necessarily) the same for all species, but reflects the differences in the formation and destruction pathways of the various species. 3) HD depletion can ultimately lead to a strong decrease of deuterium fractionation at high density, which is observed in Fig. 3.2 not only as a drop of the HD abundance at late times, but also as an eventual (abrupt) drop in the D/H abundance ratios of other species. See Paper III for details on this issue.

In conclusion, the inclusion of deuterium in a chemical model is not expected to change the abundances of undeuterated species significantly, except at very high density. However, including deuterated species makes a model more versatile by increasing the amount of viable tracer species, which is particularly important for observations toward the centers of dense cores. This issue is further discussed in Chapter 6.
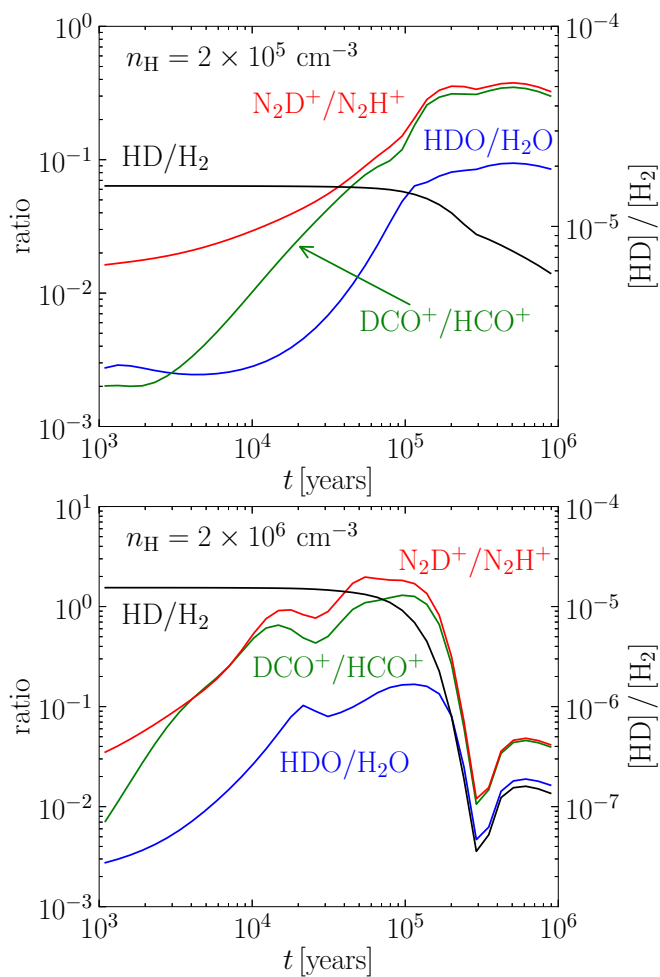
Figure 3.2: The abundance ratios of the deuterated and undeuterated forms of selected species (indicated in the figure; left y-axis) and the HD/H_2 ratio (right y-axis) as functions of time at two different densities.

Chapter 4

Spin-state chemistry

The reactions (3.1) that initiate deuterium chemistry are sensitive to the nuclear spin states of the various species involved. The part of dense core chemistry dealing with the nuclear spin states of the various species is discussed in this chapter, and is referred to as spin-state chemistry.

As an example, consider the simplest molecule, H_2, which consists of two protons with spin $1/2$ (and of two electrons). The H_2 molecule can exist in two different spin configurations, corresponding to different symmetries of the spin wave function. The *ortho* configuration corresponds to symmetric spin wavefunctions (with total nuclear spin I = 1, a triplet), while the *para* configuration corresponds to antisymmetric spin wave functions (I = 0, a singlet). The chemically relevant distinction between these two configurations is an "extra" $\sim 170\,\mathrm{K}$ worth of internal energy carried by the lowest energy state of ortho-H_2 compared to para-H_2, the importance of which is discussed below. Also, other species with multiple protons – or deuterons – such as H_3^+, D_3^+, water and ammonia, may exist in different spin configurations.

In this chapter, we review spin-state chemistry starting with a more detailed discussion of the spin states of H_2 and those of other species relevant to the thesis; we also discuss how the various chemical reactions taking place in dense cores can be "separated" so that spin-state chemistry can be included in the chemical model.

4.1   The spin states of H_2 and H_3^+

As outlined above, H_2 can exist in two distinct spin configurations, labeled ortho and para. According to the Pauli exclusion principle, the total wave function must be antisymmetric for a system consisting of two identical fermions. Therefore para-H_2 (antisymmetric spin wave function) can only have symmetric rotational wave functions ($J = 0, 2, 4, ...$, where J is the rotational angular momentum quantum number), and ortho-H_2 (symmetric spin wave function) can only have antisymmetric rotational wave functions ($J = 1, 3, 5, ...$). The $J = 1$ state lies $\sim 170\,\mathrm{K}$ above the rotational ground state with $J = 0$ (Le Bourlot 1991; Hugo et al. 2009). Because H_2 is a homonuclear molecule and thus does not have a permanent dipole moment, rotational dipole transitions with $\Delta J = \pm 1$ are forbidden and this in turn means that ortho-H_2 (hereafter $H_2(o)$) is a reservoir of energy in dense cores.

So how can $H_2(o)$ be created in dense cores, despite the fact that the internal energy of the $J = 1$ state is so high compared to the typical ambient temperature? In

the gas phase, $H_2(o)$ and $H_2(p)$ are transformed into each other mainly in the proton exchange reaction

$$H_2(p) + H^+ \longleftrightarrow H_2(o) + H^+ \, ; \qquad (4.1)$$
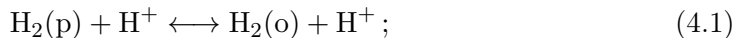
below $\sim 20\,\mathrm{K}$, however, the forward reaction loses importance because of its endothermicity (Flower et al. 2006b). Owing to the inefficiency of reaction (4.1) in the forward direction, $H_2(o)$ must instead be formed on grains. The ratio at which the ortho and para states are produced in the $H + H$ surface association depends on how the reaction is assumed to proceed; possible ortho-to-para outcomes are 3:1 (the ratio of the statistical weights) or 1:1, which occurs is the H_2 molecule is released from the grain before nuclear spin rearrangement and if the spins of the H atoms are initially random (Le Bourlot 1991). The former outcome is favored in the literature owing to the exothermicity of the $H + H$ reaction (e.g. Flower et al. 2006b; Pagani et al. 2009; Taquet et al. 2013), and is also supported by recent experiments by Watanabe et al. (2010). Also in this thesis, the 3:1 formation ratio is assumed. Because of the role of the $H + H$ surface reaction as the main mechanism of $H_2(o)$ creation and the endothermicity (in the forward direction) of the gas-phase proton exchange reaction (4.1), the H_2 ortho/para (hereafter o/p) ratio becomes non-thermal at low temperature.

The importance of the $170\,\mathrm{K}$ worth of energy in $H_2(o)$ compared to $H_2(p)$ becomes even clearer when considering the chemistry of the trihydrogen cation H_3^+, which consists of three protons and can also be separated into ortho and para forms (whose energy difference is $\sim 33\,\mathrm{K}$; Hugo et al. 2009). However, even though H_3^+ is created through the cosmic ray ionization of H_2 and the subsequent $H_2^+ + H_2$ reaction (see Sect. 2.2), its o/p ratio does not follow that of H_2. This is because reaction (2.6) creates mainly $H_3^+(p)$ (owing to the much larger abundance of $H_2(p)$ with respect to $H_2(o)$), while $H_3^+(o)$ is (mainly) created from $H_3^+(p)$ in the proton-exchange reaction

$$H_3^+(o) + H_2(p) \longleftrightarrow H_3^+(p) + H_2(o) \, . \qquad (4.2)$$
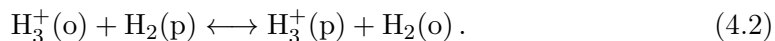
This reaction is endothermic in the forward direction by $137.6\,\mathrm{K}$ and thus negligible at $10\,\mathrm{K}$ (Flower et al. 2006b). However, because of the internal energies associated with the ortho states of H_2 and H_3^+, the reverse reaction is exothermic and can occur efficiently in dense cores. It follows that at low temperatures, the o/p ratio of H_3^+, like that of H_2, is non-thermal. We return to this issue later.

As discussed in Chapter 3, H_3^+ can be deuterated in exothermic reactions with HD (see reactions 3.1). Similarly to reaction (4.2), each of the deuteration reactions (3.1) can occur in the reverse direction when suitable spin states are involved so that the endothermicity of the reaction can be overcome. Consequently, the abundance of $H_2(o)$ is one of the most important factors controlling deuteration in dense cores. This issue is illustrated in the left panel of Fig. 4.1, where the abundance ratios of the deuterated and undeuterated forms of N_2H^+, HCO^+, and H_2O are plotted in constant physical conditions ($n_H = 2 \times 10^5\,\mathrm{cm}^{-3}$, $T_{\mathrm{gas}} = T_{\mathrm{dust}} = 10\,\mathrm{K}$) but varying the initial H_2 o/p ratio. The initial values of 3.6×10^{-7} and 3.0 for the H_2 o/p ratio represent extreme cases; the former is the abundance ratio in thermal equilibrium at $10\,\mathrm{K}$, while the latter is the ratio of the statistical weights of the ortho and para (ground) states. Evidently, a high initial abundance of $H_2(o)$ causes a delay in the development of deuterium chemistry by causing reactions (3.1) to proceed in the backward direction, reducing the abundances of the deuterated forms of H_3^+ and at
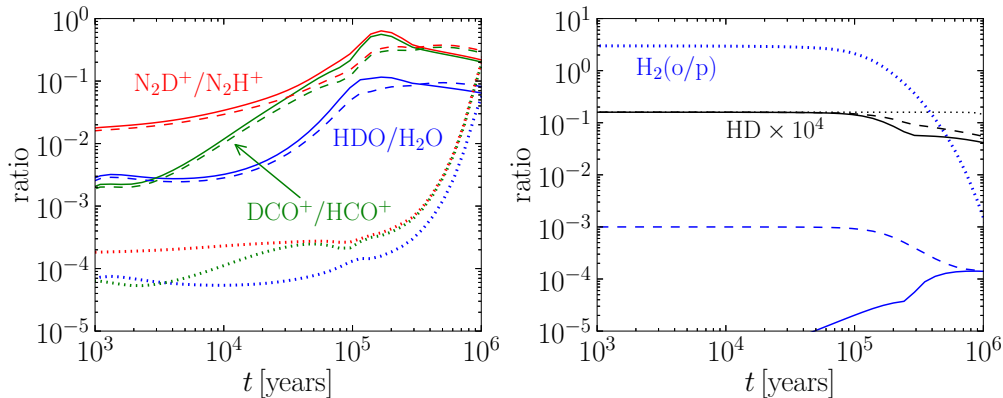
Figure 4.1: *Left:* The abundance ratios of the deuterated and undeuterated forms of selected species (color-coding indicated in the figure) as functions of time assuming an initial H_2 o/p ratio of 3 (dotted lines), 1.0×10^{-3} (dashed lines) and 3.6×10^{-7} (solid lines). *Right:* The H_2 o/p abundance ratio and the HD abundance (n_{HD}/n_H) multiplied by 10^4 as functions of time. The dotted, dashed and solid lines correspond to initial H_2 ortho/para ratios of 3.0, 1.0×10^{-3} and 3.6×10^{-7}, respectively. The physical conditions are the same in both panels; $n_H = 2 \times 10^5 \, \mathrm{cm}^{-3}$ and $T_{gas} = T_{dust} = 10 \, \mathrm{K}$.

the same time regenerating the abundance of HD. The same phenomenon is also observed in the right panel of Fig. 4.1, where the HD abundance stays constant for an extended period until it starts to deplete at $\sim 10^6$ years (barely visible in the figure). If the initial abundance of H_2(o) is low, deuteration proceeds faster and HD depletes from the gas phase at a relatively short timescale (see Paper III for an extensive discussion of HD depletion).

4.2 The spin states of the deuterated forms of H_3^+

The deuterated forms of H_3^+ also have ortho and para (and in the case of D_3^+, also meta) states, and the relative populations of the spin states are controlled by deuterated analogues of proton-exchange reactions such as (4.2). These reactions form a complicated "ladder" along which the spin-state chemistry proceeds. In what follows, we describe the most important processes controlling the spin-state abundances of H_2D^+, D_2H^+, and D_3^+ at low temperature. All of the data quoted below pertaining to rate coefficients and exo/endothermicities is from Hugo et al. (2009).

The o/p ratio of H_2D^+ is mainly controlled by the proton-exchange reaction

$$H_2D^+(p) + H_2(o) \longleftrightarrow H_2D^+(o) + H_2(p) \tag{4.3}$$
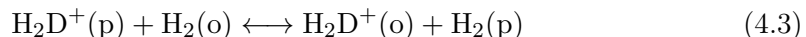
in the forward direction (the reverse reaction is endothermic by about $80 \, \mathrm{K}$) – other similar reactions between the various spin states of H_2D^+ and H_2 are either endothermic or have lower α coefficients. Based on this fact, we expect the H_2D^+ (o/p) ratio to increase toward lower temperatures, which is indeed predicted by chemical models (e.g. Papers I and III).

D_2H^+ is interesting in the sense that the proton-exchange reactions with H_2 that interconvert D_2H^+(p) and D_2H^+(o) are forbidden by quantum mechanical selection
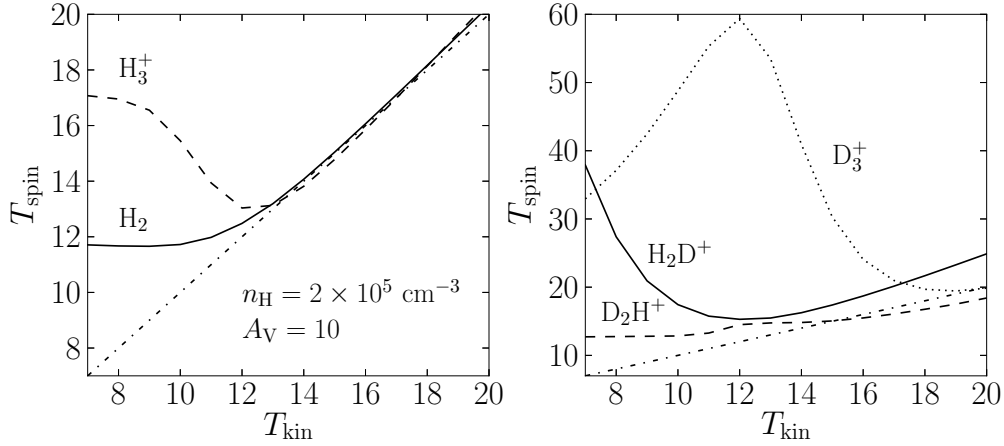
Figure 4.2: *Left:* The spin temperatures of H_2 (solid line) and H_3^+ (dashed line) as functions of the kinetic temperature. *Right:* The spin temperatures of H_2D^+ (solid line), D_2H^+ (dashed line) and D_3^+ (dotted line) as functions of the kinetic temperature. In both panels, $T_{\mathrm{spin}} = T_{\mathrm{kin}}$ is depicted as a dash-dotted line to help guide the eye.

rules, while similar reactions with HD and D_2 are not. Of the allowed reactions, those that convert $D_2H^+(o)$ to $D_2H^+(p)$ are endothermic – therefore, one expects to find more $D_2H^+(o)$ than $D_2H^+(p)$ at low temperatures. Modeling indicates that this is indeed the case (Flower et al. 2004; Papers I and III).

D_3^+ has three spin configurations, of which the para form lies highest in energy and is the least populated in dense cores; therefore, we concentrate here on the meta/ortho (m/o) ratio. Just like for D_2H^+, the spin-state conversion reactions $D_3^+ + H_2$ are forbidden, and the spin-state balance is controlled mainly by reactions with HD and D_2. Meta-to-ortho conversion reactions are mostly endothermic, so that one expects (m/o) > 1 at low temperatures (Flower et al. 2004; Papers I and III – note that the meta and ortho appelations in Flower et al. are reverse to what is used here).

It should be noted that the spin-state balance is influenced not only by the proton-exchange reactions quoted above, but also to some extent by the formation/destruction reactions (3.1). The dependences of the spin-state abundances on density and on grain radius are generally weak, but non-trivial (Flower et al. 2004; Paper I). Therefore, it is usually very difficult to draw qualitative conclusions about the spin-state abundances for a given a set of physical parameters, and detailed chemical modeling is required. This issue becomes important when observations are analyzed (see Chapter 6).

4.3 Illustrating the spin-state abundance ratios

The temperature-dependence of the spin-state abundance ratios of the various species can be illustrated not only by directly plotting the ratio (as is done in the papers referenced above), but also by using the *spin temperature*, defined assuming a Boltzmannian distribution of the energy levels:

$$\frac{n_{\mathrm{u}}}{n_{\mathrm{l}}} = \frac{g_{\mathrm{u}}}{g_{\mathrm{l}}} \exp\left(-\frac{\varepsilon_{\mathrm{ul}}}{k_{\mathrm{B}}T_{\mathrm{spin}}}\right) , \qquad\qquad (4.4)$$

where n_i is the population of energy level i, g_i is the statistical weight (including possible degeneracy) of the energy level and ε_{ij} is the energy separation between the two levels (i.e. 170 K in the case of H_2)[1]. According to this definition, a spin-state abundance ratio higher than the thermal equilibrium value corresponds to $T_{spin} > T_{kin}$. To illustrate the non-thermal nature of the spin-state distributions at low temperatures, the spin temperatures of H_2 and H_3^+ are plotted in the left panel of Fig. 4.2 at constant density and visual extinction as functions of the kinetic temperature ($T_{kin} = T_{gas} = T_{dust}$), while the right panel of the figure plots the spin temperatures of H_2D^+, D_2H^+, and D_3^+. Evidently, the spin-state abundance ratios of all the plotted species are super-thermal at low T_{kin}. Furthermore, the spin temperatures of the deuterated forms of H_3^+ can be non-thermal even at 20 K. This fact further underlines the importance of chemical modeling for the interpretation of observations.

4.4 Inclusion of spin-state chemistry in the chemical model

It is evident from all of the above that the $H_3^+ + H_2$ reacting system plays a large role in the progression of deuterium chemistry (cf. reactions 3.1). Therefore, the treatment of this system is an integral part of any chemical model including deuterium and/or spin-state chemistry. Indeed, the importance of the $H_2D^+ + H_2$ system was described already ~ 20 years ago by Pagani et al. (1992). Subsequently, Walmsley et al. (2004) and Flower et al. (2004) (hereafter, we refer to these two publications together as WF04) published an extensive analysis of the $H_3^+ + H_2$ reacting system including also D_2H^+ and D_3^+ and their respective spin-state chemistries, in a model where all heavy elements are depleted onto grain surfaces (the "complete depletion" model). These authors presented the rate coefficients of not only the $H_3^+ + H_2$ reacting system, but also of other important (e.g. charge transfer, proton exchange) reactions between light species (up to He), including recombinations of cations with electrons and grains (see also Flower & Pineau des Forêts 2003).
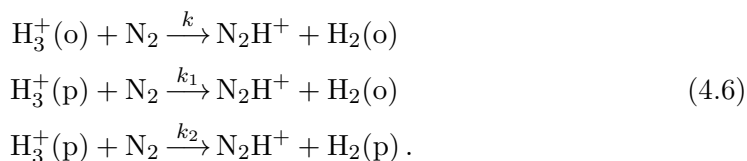
The branching ratios pertaining to the various reactions in the $H_3^+ + H_2$ system presented by WF04 are based on a statistical description and depend on how the reactions are assumed to proceed; that is whether, e.g., $H_3^+ + HD$ proceeds by H-D exchange or by proton-donation. The α coefficients assumed by WF04 for these reactions are from Gerlich et al. (2002). Recently, Hugo et al. (2009) derived the state-to-state rate coefficients pertaining to the $H_3^+ + H_2$ reacting system, including all of the deuterated forms and spin states, using a microcanonical approach based on phase-space theory. In their work, the nuclei are completely scrambled in the reaction and the resulting state-to-species rate coefficients are generally different by a factor of a few, and sometimes even by an order of magnitude, than those given by WF04 for the corresponding reactions. In Paper I, we studied the complete depletion model adopting the Hugo et al. (2009) rate coefficients for the $H_3^+ + H_2$ system and found that deuteration proceeds much faster when one adopts the Hugo et al. (2009) coefficients compared to those used by WF04, and that the spin-state abundances are also modified (see Paper I for a detailed discussion of this issue).

---

[1]The use of formula (4.4) for defining the spin temperature is generally fine in the context of dense core chemistry, because the low ambient temperature ensures that only the lowest energy levels are significantly populated.

In the present version of the chemical model developed in this thesis (most recently used in Paper III), the deuterium and spin-state chemistry involving the light species is taken from the chemical reaction network used in Paper I, which is a combination of data from WF04, Hugo et al. (2009) and Pagani et al. (2009). To include the spin-state chemistry related to reactions between the light species and more massive species containing heavy elements (C, N, O etc.), an automated routine was designed for Paper III to "separate" these reactions (originating in the OSU reaction set) to account for spin-state chemistry. For example, the reaction

$$H_3^+ + N_2 \xrightarrow{k} N_2H^+ + H_2 \qquad (4.5)$$

separates into the following three reactions when spin states are taken into account:

$$
\begin{aligned}
H_3^+(o) + N_2 &\xrightarrow{k} N_2H^+ + H_2(o) \\
H_3^+(p) + N_2 &\xrightarrow{k_1} N_2H^+ + H_2(o) \\
H_3^+(p) + N_2 &\xrightarrow{k_2} N_2H^+ + H_2(p) \, .
\end{aligned}
\qquad (4.6)
$$

Why the first reaction can only produce $H_2(o)$ can be explained as follows. $H_3^+(o)$ consists of three protons with aligned spins and hence removing one proton from the system necessarily results in H_2 with both proton spins aligned (the ortho form) – provided that the total spin is conserved in the reaction. The values of k_1 and k_2 in the two latter reactions, i.e., the branching ratios, cannot on the other hand be trivially deduced. To calculate the branching ratios in reactions such as (4.6), we have used the method of Oka (2004), which uses angular momentum algebra to derive selection rules for reactive collisions. This method yields $k_1 = k_2$ for reaction (4.6), i.e., a 1:1 branching ratio, so that $k_1 = k_2 = k/2$. For simplicity, we have assumed that all reactions similar to (4.6) yield a 1:1 branching ratio when $H_3^+(p)$ is involved in the reaction.

There are many reaction types for which the above branching ratios cannot be assumed. For example in charge-transfer reactions, no nuclei are exchanged between the reactants, and consequently the ortho/para states are assumed to be conserved. The various special cases are listed in Appendix A of Paper III, where we also discuss the assumptions made in separating each reaction type. It is recognized that the various assumptions regarding the branching ratios may introduce a certain amount of error into the model – however, such error is most likely small compared to typical uncertainties in the rate coefficients themselves.

Finally we note that in addition to H_2 and H_3^+, also other species with multiple protons, such as water and ammonia, exist in ortho and para states, and for example the spin-state chemistries of ammonia and C_3H_2 have been studied in the literature (respectively: Flower et al. 2006a; Park et al. 2006). The inclusion of the spin states of heavier species presents a possible avenue for the expansion of the chemical model.

Chapter 5

The chemical model program *pyRate*

All of the chemical calculations for the papers included in this thesis have been carried out using a chemical model program called *pyRate* written in the Python language, developed in-house at the University of Helsinki. In short, pyRate solves a system of coupled first-order differential equations (DEs) constructed according to the rate equation method, and includes the various gas-phase and grain-surface reaction mechanisms discussed in the previous chapters.

The first (gas-phase chemistry only) version of pyRate was written by M. Juvela, but after the beginning of the thesis work (late 2008), the present author has been responsible for the development of the program.

5.1   How pyRate works

This section outlines the features of pyRate, following the progression of a typical program run.

Initialization

Before any calculations are performed, a host of parameters are loaded into the program from an initialization file. The physical parameters required by the program are listed in Table 5.1 along with a description. In addition to the physical parameters, the program reads from the same initialization file the values of other keywords such as whether adsorption/desorption or quantum tunneling are to be included in the calculation. The filenames for external data (reaction sets with the associated rate coefficient parameters, binding energies etc.) are also declared here.

If not read from an external file declared by a keyword, the abundance of grains is calculated internally in the program, following the equation presented in Sect. 2.2.2. It is usually assumed that all grains are initially neutral.

Construction of gas-phase reactions

In the gas-phase reaction files read by pyRate, the reaction entries (one line per reaction) are formatted as follows:

Table 5.1: The physical parameters required by pyRate.

Parameter	Description
T_gas	The gas temperature
T_dust	The dust temperature
ζ	The cosmic ray ionization rate
A_V	The visual extinction
ω	The grain albedo
a_g	The grain radius
n_H	The total hydrogen density
ρ_g	The grain material density

```
424 H+ H2S H2S+ H 3.80e-09 -0.50 0.00 0.0 0.0
```

Here, the integer in the front is the index of the reaction (for bookkeeping purposes only, not used by the program). Next, the two reactants and the 1-4 reaction products are defined. The three following floating point numbers represent the α, β and γ coefficients, respectively, used to construct the rate coefficient of the reaction. Finally, the two numbers at the end of the line represent the temperature range where the rate coefficient is valid (0.0, 0.0 means that the rate coefficient is, supposedly, valid at any temperature).

pyRate scans the reactions one at a time and decides based on the reactants which form of the rate coefficient should be used, and calculates the rate coefficient. Finally, each reaction is stored as a Python list as [[list of reactants], [list of products], rate coefficient].

Construction of adsorption and/or desorption "reactions"

The adsorption and/or desorption processes, if specified in the initialization file to be included in the calculation, are defined internally in the program. For each neutral species included in the calculation, pyRate constructs the adsorption and/or desorption rate coefficients according to the formulae presented in Chapter 2, and appends the resulting "reactions" to the complete list of reactions.

Construction of grain surface reactions

If surface reactions are to be included, the program reads the reaction data from a surface reaction file formatted similarly to the gas-phase reaction file. The rate coefficient of each reaction is then calculated by determining the diffusion rates of the reactants and the reaction probability based on the possible activation energy of the reaction. Finally, the surface reactions are appended to the complete list of reactions.

Solving the chemical evolution

After all reactions and the associated rate coefficients have been determined, the program proceeds to construct the formation and destruction rates of each species by summing over all of the formation and destruction pathways, respectively.

The formation and destruction rates of each species are subtracted from each other to form the time derivative of the density of the species (see Chapter 2). Solving the overall chemical evolution thus becomes a problem of solving a system of coupled first-order DEs.

The system of DEs is solved using `odeint` (which uses `LSODA` from `odepack`), a DE solver distributed as part of the open-source `SciPy` library. The `YDOT` object representing the system of differential equations is written as a `C` language subroutine into an external file, compiled, and then imported back to pyRate for `odeint` to use. The reason for using `C` in this context is that this method is much faster than the purely Python-based alternative.

Output

After the system of DEs is solved, `odeint` outputs an $n \times m$ matrix, where n is the number of time steps and m is the number of species; the matrix elements are written into a result file so that each column represents the time-evolution of a single species. Optional output includes, for example, plotting and checking of elemental balance. Perhaps the most useful optional output is produced by an analysis function that writes into a file the main formation and destruction reactions and the associated reaction rates for each desired species at any desired time, so that the relative importance of the various reactions can be easily assessed.

5.2 Performance

Because of the relative simplicity of the problem at hand, i.e., solving a system of ordinary first-order DEs, a typical pyRate run takes only a few minutes depending mainly on the size of the reaction network; increasing the amount of reactions increases the time the solver uses for matrix inversion. The physical parameters also influence the runtime somewhat, as they contribute to the stiffness of the problem. For example, a run using the full reaction sets of Paper III (including deuterium and spin-state chemistry, about 13000 reactions in total) takes about 2 minutes on a standard desktop computer (on a single core; pyRate is not designed for multicore calculations). Of the total runtime, about 10 seconds is spent on initialization and compiling the `C` subroutine, and the rest is spent on solving the DEs.

5.3 The implementation of pyRate in dense core modeling

pyRate is designed to calculate chemical evolution for a single set of physical parameters (e.g. density and temperature) so that the result of any calculation refers to a single point in a core model. However, in a real dense core the physical parameters vary with radial distance from the core center, and consequently the timescales of the various chemical processes are different in each point in the core. To model the chemical structure of dense cores with pyRate, one must therefore run the program for a series of physical conditions. The radial abundance profiles presented in the papers included in this thesis were produced by looping over a set of physical conditions varying with radius – that is, in between model runs, the initialization file was updated with a new set of physical parameters. Finally, the abundances of each

desired species corresponding to a given time were extracted from the result files and combined to yield radial abundance profiles. This pseudo-time-dependent approach is fine if the core is assumed to be static in the sense that the physical conditions do not change during the course of the chemical evolution and there is no material exchange between different parts of the core.

However, as also noted in Sect. 2.3, in a realistic situation the gas temperature can be expected to change as the abundances of the main cooling species evolve. This issue was simulated in Papers II and III by adopting an iterative approach: the abundance profiles resulting from initial chemical calculations were used as input for a radiative transfer program to determine the gas temperature, after which the chemical abundances were recalculated using the new temperature profile. The process was repeated a few times until both the chemical abundances and the gas temperature converged. This semi-self-consistent approach in which the density profile does not change was adopted so that a more realistic descprition of the core temperature profile could be achieved (as this affects observable line emission) – it should be noted that, realistically, a change in the gas temperature should also change the density profile through changes in thermal pressure (see also Chapter 7).

5.4 Future development of pyRate

pyRate can be developed further to describe additional chemical processes. These include, but are not limited to, photodesorption, multilayer (mantle + separate surface layer) grain-surface chemistry, porosity and chemisorption. To better account for surface chemistry on small grains, modifications to the rate equation method (Caselli et al. 1998; Garrod 2008; Du & Parise 2011) could be made. We note that rudimentary descriptions of chemisorption and of the modified rate equation method already exist in the program, but these are largely untested.

With appropriate adjustments to the way the DEs are solved, that is to move from a pseudo-time-dependent model into a fully time-dependent model, pyRate could be combined with, e.g., an (M)HD code for chemical calculations in varying physical conditions to model for example the chemistry during core collapse. Similar calculations have been carried out in the literature (e.g. Aikawa et al. 2012).

Chapter 6

Simulated observations of dense cores

A chemical model is merely a curiosity unless its predictions can be compared against observations. Such a comparison can be carried out in multiple ways. For example, radial molecular abundances predicted by a model can be converted to column densities to be compared with those deduced from observations. Another approach is to simulate line emission radiation by combining the chemical model with radiative transfer calculations, and to compare the simulated spectra directly against observed ones. The latter approach was followed in Papers I and V.

In this chapter, we discuss the line emission simulations carried out in this thesis. We begin by introducing the concept of line emission. We then discuss tracers of the central areas of dense cores, focusing on H_2D^+ and D_2H^+, and finish with a discussion on how the line emission simulations of Paper I would be affected if we used instead the new chemical model developed for Paper III.

6.1 The concept of line emission

The various chemical species present in dense cores can be excited to higher energy levels by, e.g., irradiation by external photons incident on the core, or in collisions with one another. Quantum mechanics tells us that the energy levels are discrete, and that the separations between the various energy levels are fixed by the properties of the species. Relaxation back into lower energy levels produces observable photons, and it can be shown that the intensity profile of the radiation produced in the relaxation takes the form of a spectral line (e.g. Dyson & Williams 1997).

At the low temperatures of dense cores, electronic excitation does not occur efficiently and only the lowest rotational levels of the various species are significantly populated. In the case of diatomic molecules such as H_2, the energies of the rotational levels are given (in the rigid rotor approximation) by

$$E_J = B\,J\,(J+1)\;,\qquad\qquad\qquad (6.1)$$

where $J = 0, 1, 2...$ is the rotational quantum number describing angular momentum and $B = \hbar^2/2I$ is the rotational constant; $I = \mu r^2$ is the moment of inertia of the species. Thus, the more massive the species, the closer the separation between the rotational energy levels. For nonlinear species, more quantum numbers are needed

(which is the case for, e.g., H_2D^+ and D_2H^+) and the mathematical form of E is somewhat more complicated.

The frequency of the photon emitted in a transition is related to the energy separation between the two levels associated with the transition by $\Delta E = h\nu$. Equation (6.1) thus indicates that the frequency of the photon emitted in the transition *in situ* is affected only by the properties of the emitting species.

Various factors however affect the frequency of the *observed* line emission radiation, which is a combination of the lines emitted by a large amount of molecules. In general, the observed object is moving with respect to the observer, which induces a shift in the line frequency because of the Doppler effect. Furthermore, the more or less random velocities of the various molecules in a given line of sight toward the observed object broaden the line (collisional broadening is usually unimportant; Dyson & Williams 1997). For these reasons, radiative transfer modeling of the emission is needed to understand the observations – chemical modeling is needed to study the initial condition for radiative transfer, i.e., the amount of emitting molecules in the line of sight.

6.2 Potential tracers of the central areas of dense cores

Different chemical species probe different areas of dense cores. For example, species containing carbon and/or sulphur, such as CO, CS, and SO, are expected to be strongly depleted at high density (e.g. Tafalla et al. 2006; Stahler & Yen 2010; Paper II). Consequently, the line emission by these species coming from the centers of dense cores is very weak, so that these species can only be used to probe the outer, less dense, areas of the cores. On the other hand, N_2H^+ for example is expected to resist depletion, and can trace also the innermost areas of the cores (Tafalla et al. 2002; Flower et al. 2006a; Paper II).

Deuterium plays an important role in observations of the central areas of dense cores. The deuterated form of a given species can in some cases probe further into a core than the non-deuterated counterpart owing to strong deuterium fractionation; this effect has been observed for example for HCO^+ (Tafalla et al. 2006). Deuterium fractionation also gives rise to two important tracer species: H_2D^+ and D_2H^+. Because of the central role of these two species in the line emission simulations performed in this thesis (Paper I), we next discuss them in more detail.

6.3 H_2D^+ and D_2H^+ as tracer species

The trihydrogen cation H_3^+, just like H_2 discussed earlier, consists of identical nuclei and does not possess a permanent dipole moment. Consequently, rotational dipole transitions are forbidden and H_3^+ cannot be detected in emission toward dense cores. Its deuterated forms H_2D^+ and D_2H^+ however possess relatively easily excitable (ground-state) rotational transitions and thus these species are detectable toward dense cores also in emission. Not all of the spin states are detectable from the ground, however. Table 6.1 summarizes the frequencies of the ground-state transitions of ortho and para H_2D^+ and D_2H^+. Of these four ground-state transitions, those of H_2D^+(p) and D_2H^+(o) are inaccessible from the ground owing to their frequencies (the atmosphere is opaque at these frequencies).

Table 6.1: The frequencies of the ground-state rotational transitions of ortho and para H_2D^+ and D_2H^+. Data from Amano & Hirao (2005).

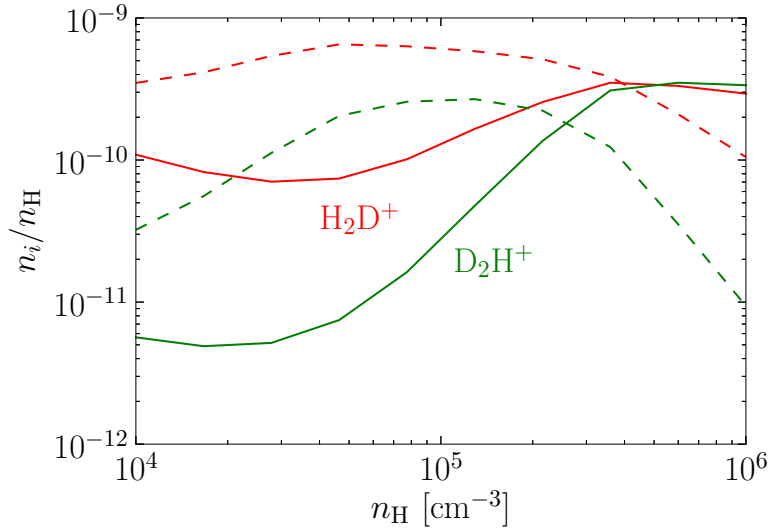| Species	Transition	Frequency
H_2D^+(p)	$1_{01} - 0_{00}$	1.370 THz
H_2D^+(o)	$1_{10} - 1_{11}$	372.4 GHz
D_2H^+(p)	$1_{10} - 1_{01}$	691.6 GHz
D_2H^+(o)	$1_{11} - 0_{00}$	1.477 THz

Figure 6.1: The abundances of (ortho+para) H_2D^+ and D_2H^+ (color-coding indicated in the figure) as functions of density at $t = 1 \times 10^5$ years (solid lines) and at $t = 5 \times 10^5$ years (dashed lines).

The ground-state transitions of H_2D^+(o) and D_2H^+(p) are however detectable from the ground. H_2D^+(o) was first detected in the ISM by Stark et al. (1999) toward the low-mass protostar NGC1333 IRAS 4A; the first detection toward a dense core was published by Caselli et al. (2003). The transition has been subsequently detected toward many different dense cores (e.g. Vastel et al. 2006; Caselli et al. 2008; Harju et al. 2008). D_2H^+(p) is hard to detect because of its weak emission (see below), and only two detections have been achieved to this day (Vastel et al. 2004; Parise et al. 2011).

H_2D^+ and D_2H^+ are formed most efficiently in the centers of dense cores, because their formation requires the depletion of abundant heavy molecules such as CO (see Chapter 3). However, this statement just implies that the timescale for the formation of these species is shortest at high density. The formation of H_2D^+ and D_2H^+ can proceed also at lower densities and hence one could expect extended abundance profiles for these species (Paper III). This fact is demonstrated in Fig. 6.1, where the abundances of H_2D^+ and D_2H^+ (as sums of their respective ortho and para states) are plotted as functions of density at two different times. The temperature is set to $T_{gas} = T_{dust} = 10$ K at each density. The time-dependence of the deuterium chemistry

is evident here: at $t = 1 \times 10^5$ years, both abundance profiles are centrally peaked while at $t = 5 \times 10^5$ years, the abundance maxima lie close to $n_{\mathrm{H}} \sim 10^5\,\mathrm{cm}^{-3}$ because HD depletion decreases deuterium fractionation at high density (Paper III). The figure also shows that both species may have extended abundance profiles especially at late times. Indeed, extended spatial distributions have been observed for both $H_2D^+(o)$ (Vastel et al. 2006; Pagani et al. 2009) and $D_2H^+(p)$ (Parise et al. 2011).

The observed distributions, while extended, are still centrally peaked. In light of Fig. 6.1, one is tempted to think that this is an indication that the cores are young. Because of the limited angular resolution of the observations, however, it is hard to discriminate the very small high density nucleus of the core (if such exists) from the surrounding gas and thus a volume where deuterium fractionation is decreased due to HD depletion may be generally missed by observations. Rather, the peak of observed intensity may generally be associated with gas with $n_{\mathrm{H}} \sim 10^5\,\mathrm{cm}^{-3}$. We note that to study this issue, accurate observations combined with very detailed modeling of each observed core would be needed, and that such a study would be desirable for the development (and validation) of chemical models.

6.4 Line emission simulations: comparison between Paper I and Paper III

In Paper I, we carried out simulations of $H_2D^+(o)$ and $D_2H^+(p)$ line emission, using the state-to-state rate coefficients of Hugo et al. (2009). The chemical model used in Paper I considers gas-phase chemistry, and the only grain-surface reactions included are the formation of H_2, HD, and D_2. Heavy elements are not included, and hence HD depletion does not occur. As the density and temperature profiles studied in Paper I correspond to a high-density core nucleus where time-dependent depletion effects should be important, it is instructive to reconsider the line emission simulations of Paper I in the context of the new model developed for Paper III.

To demonstrate this issue, simulated spectral line profiles of the $H_2D^+(o)$ $1_{10}-1_{11}$ transition and the $D_2H^+(p)$ $1_{10}-1_{01}$ transition are shown in Fig. 6.2, using either the chemical model of Paper I or that of Paper III. For these calculations, the physical core model of Paper I with grain radius $a_{\mathrm{g}} = 0.1\,\mu\mathrm{m}$ was adopted (see Fig. 5 in Paper I). Evidently, the simulated emission is very sensitive to time owing to time-dependent depletion effects, and at $t = 10^6$ years the D_2H^+ line is virtually undetectable. Emission is in general weaker in the new model because of lower H_2D^+ and D_2H^+ abundances compared to the model of Paper I.

In conclusion, the chemical model of Paper III will not reproduce the simulation results of Paper I – if the same physical parameters are assumed. This fact underlines a basic problem with line emission simulations: an observed line profile can often be fitted rather well by simply tuning the various model parameters. Often the freedom for parameter tuning is great, as there are seldom many different kinds of observations toward a single object that would simultaneously constrain, for example, the density profile, the grain properties (grain material, size distribution etc.) and the temperature. Therefore, a model should be required to 1) fit the available observations and 2) predict new observable results based on these fits – if the predicted results are confirmed by subsequent new observations, one can say that the model stands on firmer ground.
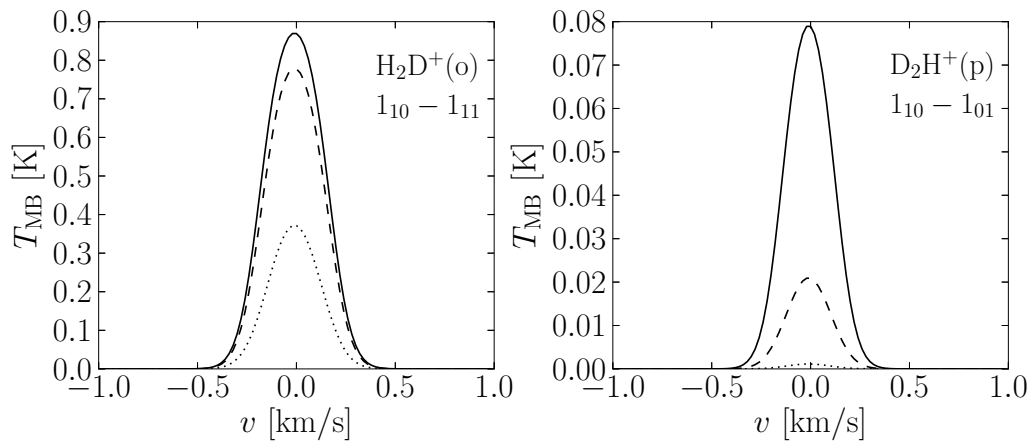
Figure 6.2: *Left:* Simulated emission of the $H_2D^+(o)$ $1_{10} - 1_{11}$ transition using either the chemical model of Paper I (solid line) or that of Paper III at $t = 10^5$ years (dashed line) and at $t = 10^6$ years (dotted line). *Right:* As the left panel, but modeling the $D_2H^+(p)$ $1_{10} - 1_{01}$ transition.

Chapter 7

The stability of dense cores and the connection to chemistry

When discussing chemical modeling of dense cores involving timescales longer than $\sim 10^5$ years, one should make sure that the model is also physically sound, i.e., that the model core can be expected to be dynamically stable for the duration of the chemical evolution. Dense cores are supported against gravitational collapse mainly by thermal pressure – non-thermal contributions to the stability can come from turbulence (usually subsonic, see e.g. Myers & Benson 1983; Kirk et al. 2007) and/or the magnetic field (e.g. Mestel & Spitzer 1956). Therefore, determining the gas temperature is key to understanding the core stability.

In all of the papers included in this thesis, we adopt the so-called modified Bonnor-Ebert sphere (see below) as the physical core model. In this chapter, the core model and its stability are discussed. We also briefly discuss how the stability is connected to the gas temperature, and consequently to the core chemistry.

7.1   The Bonnor-Ebert sphere

The Bonnor-Ebert sphere (Ebert 1955, Bonnor 1956; hereafter BES) is an isothermal gas sphere in hydrostatic equilibrium, bounded by external pressure. The density distribution of the BES is given by

$$\frac{1}{r^2}\frac{d}{dr}\left(\frac{r^2}{\rho}\frac{d\rho}{dr}\right) = -\frac{4\pi Gm\rho}{kT}\,,\tag{7.1}$$

i.e., a combination of the ideal gas equation of state and the equation of hydrostatic equilibrium (Bonnor 1956). Equation (7.1) can be written in non-dimensional form by making the substitutions

$$\rho = \lambda e^{-\psi}\,;\, r = \beta^{1/2}\lambda^{-1/2}\xi\,,\tag{7.2}$$

where λ is an arbitrary constant (usually chosen to correspond to the central density of the core, see below) and $\beta = kT/4\pi Gm$ represents the temperature (m is the average molecular mass of the gas). ψ and ξ are dimensionless variables. Using the substitutions (7.2), Eq. (7.1) transforms to

$$\frac{1}{\xi^2}\frac{d}{d\xi}\left(\xi^2\frac{d\psi}{d\xi}\right) = e^{-\psi}\,,\tag{7.3}$$
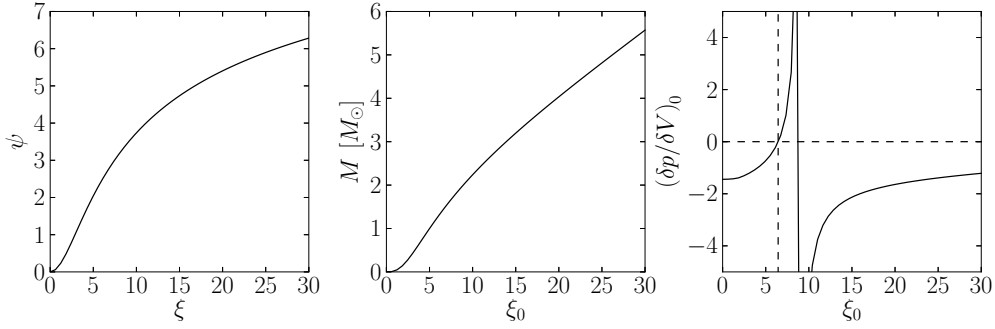
Figure 7.1: *Left:* The solution of Eq. (7.3). *Middle:* The core mass according to Eq. (7.7) as a function of the outer radius ξ_0 in units of solar mass, assuming $T = 10\,\mathrm{K}$ and $n(\mathrm{H}_2)_\mathrm{c} = 10^5\,\mathrm{cm}^{-3}$. *Right:* The pressure derivative at the core edge as a function of the outer radius ξ_0. Horizontal and vertical dashed lines have been set at $(\delta p/\delta V)_0 = 0$ and $\xi_0 = 6.451$, respectively, to help guide the eye.

which is a variant of the Lane-Emden equation. Natural boundary conditions for the solution of Eq. (7.1) are

$$\rho(r = 0) = \rho_\mathrm{c}\,;\ (d\rho/dr)_{r=0} = 0\,. \tag{7.4}$$

If we choose $\lambda = \rho_\mathrm{c}$, then the non-dimensional boundary conditions are

$$\psi(\xi = 0) = 0\,;\ (d\psi/d\xi)_{\xi=0} = 0\,. \tag{7.5}$$

With these boundary conditions, Eq. (7.3) can be solved. The solution yields ξ and $\psi(\xi)$, which can be converted back to physical variables using (7.2). Note that Eq. (7.3) depends only on dimensionless variables, and the solution is unique.

The solution of Eq. (7.3) extends to infinity, and represents an entire family of core configurations, as can be seen with the following argument. Let us first fix the temperature and central density, i.e., β and λ. Then, ψ and consequently $d\psi/d\xi$ are given by the solution to Eq. (7.3). Now, for example the mass M of a BES,

$$M = \int_0^r 4\pi y^2 \rho(y) dy\,, \tag{7.6}$$

can be written with the substitutions (7.2) as

$$M = 4\pi\beta^{3/2}\lambda^{-1/2}\int_0^{\xi_0} \xi^2 e^{-\psi} d\xi = 4\pi\beta^{3/2}\lambda^{-1/2}\xi_0^2\left(\frac{d\psi}{d\xi}\right)_0\,, \tag{7.7}$$

where we used Eq. (7.3) and the fact that β and λ are constants. The upper bound of the integral, ξ_0, represents the outer radius of each core configuration – evidently, each value of ξ_0 (and the associated $(d\psi/d\xi)_0$) yields a different core mass and thus there exists for each fixed pair (β,λ) an infinite set of core configurations with unique masses. This is illustrated in Fig. 7.1, where the left panel shows the solution of Eq. (7.3), and the middle panel shows the core mass according to Eq. (7.7) as a function of ξ in units of solar mass.

Alternatively, one can fix the temperature and the mass of the core, which then yields another series of core configurations, each with a unique central density. Note that this effectively means that λ is a function of ξ_0, while in the above we considered it as a constant! Indeed, λ can be considered constant *separately for each value of the outer radius* ξ_0.

Consider now the stability of the BES against gravitational collapse, assuming that the core is supported by thermal pressure only. The core is stable as long as an increase in internal pressure balances any contraction of the core, i.e., if the pressure derivative $\delta p/\delta V$ at the core edge is negative. The pressure and volume can be written in terms of ξ, ψ, β, and λ as

$$p = \frac{\rho k T}{m} = 4\pi G \beta \lambda e^{-\psi} \,, \tag{7.8}$$

$$V = \frac{4\pi}{3} r^3 = \frac{4\pi}{3} \beta^{3/2} \lambda^{-3/2} \xi^3 \,. \tag{7.9}$$

Using these, one can derive the mathematical form of the pressure derivative:

$$
\begin{aligned}
\frac{\delta p}{\delta V} &= \frac{4\pi G \beta}{\frac{4\pi}{3} \beta^{3/2}} \times \frac{e^{-\psi} \delta\lambda - \lambda e^{-\psi} \left(\frac{d\psi}{d\xi} \right) \delta\xi}{-\frac{3}{2} \lambda^{-5/2} \xi^3 \delta\lambda + 3\lambda^{-3/2} \xi^2 \delta\xi} \\
&= \frac{2p}{3V} \times \frac{\lambda^{-1} \delta\lambda - \left(\frac{d\psi}{d\xi} \right) \delta\xi}{2\xi^{-1} \delta\xi - \lambda^{-1} \delta\lambda} \,.
\end{aligned} \tag{7.10}
$$

The critically stable configuration is that for which $(\delta p/\delta V)_0 = 0$; this occurs at $\xi_0 \sim 6.451$ as demonstrated by the right panel of Fig. 7.1, where $(\delta p/\delta V)_0 = 0$ is plotted as a function of ξ_0. Evidently the pressure derivative turns negative again for larger values ($\gtrsim 9$) of ξ_0, but it can be shown that all configurations with $\xi_0 > 6.451$ correspond to unstable cores (Bonnor 1956). In other words, studying the stability of the BES is equivalent to finding the configuration which is critically stable; all configurations for which the non-dimensional outer radius ξ lies below the critical value are dynamically stable.

The uniqueness of the solution to Eq. (7.3) fixes the density contrast (i.e. the ratio of the densities at the core center and edge; cf. Eq. 7.2) attributed to each value of ξ_0, so that a critical BES always has a density contrast $\rho_{\mathrm{con}} = \rho_{\mathrm{c}}/\rho_{\mathrm{out}} = \exp\{-\psi(6.451)\} \sim 0.07$. For stable spheres, $\rho_{\mathrm{con}} \lesssim 0.07$.

7.2   The modified Bonnor-Ebert sphere

The modified Bonnor-Ebert sphere (Evans et al. 2001; Keto & Field 2005; hereafter MBES) differs from the BES in that it is non-isothermal, i.e., that $T = T(r)$. With this assumption, the density distribution equation takes the form

$$\frac{1}{r^2} \frac{d}{dr} \left(\frac{r^2}{\rho} \left[T\frac{d\rho}{dr} + \rho\frac{dT}{dr} \right] \right) = -\frac{4\pi G m \rho}{k} \,. \tag{7.11}$$

To transform this equation into a Lane-Emden-like dimensionless equation, the substitutions (7.2) need to be modified. One should use instead

$$\rho = \frac{\lambda}{\tau} e^{-\psi} \,;\, r = \beta^{1/2} \lambda^{-1/2} \xi \,, \tag{7.12}$$

where $\tau = T(r)/T_{\mathrm{c}} = T(\xi)/T_{\mathrm{c}}$, T_{c} is the temperature at the core center and $\beta = kT_{\mathrm{c}}/4\pi Gm$. Using these substitutions, (7.11) becomes

$$\frac{1}{\xi^2}\frac{d}{d\xi}\left(\xi^2\tau\frac{d\psi}{d\xi}\right) = \frac{1}{\tau}e^{-\psi}, \tag{7.13}$$

which can be solved by adding $\tau(\xi = 0) = 1$ and $(d\tau/d\xi)_{\xi=0} = 0$ to the boundary conditions (7.5). The solution of Eq. (7.13) and the stability of the MBES are extensively studied in Paper IV.

7.3 The connection of chemistry to core stability

Because thermal pressure is the main stabilizing factor in dense cores, the gas temperature plays a critical role in determining whether a core is stable. In Paper IV, the stability of the MBES was studied assuming $T_{\mathrm{dust}} = T_{\mathrm{gas}}$, which is however valid only when density is high ($n_{\mathrm{H}} \gtrsim 10^5\,\mathrm{cm}^{-3}$). At lower densities, where collisional coupling between the gas and the grains is weak, the cooling of the gas – and hence the gas temperature – is determined by molecular abundances and T_{gas} falls below T_{dust} (if the core is sufficiently shielded from external radiation; e.g. Keto & Field 2005; Juvela & Ysard 2011; Paper II). Therefore, in a realistic scenario, the thermal pressure at low density is likely to be lower than what is assumed in Paper IV, and this may have implications on the stability of high-mass MBESs in particular because these cores have low average density (see Paper IV).

Because the stability is in Paper IV determined by the dust temperature, there are no time-dependent effects present (the dust temperature is assumed not to evolve with time). However, when considering the gas temperature as the source of thermal stability, the situation changes because the gas temperature is a function of time (e.g. Paper II). This leads to an interesting question: could a stable core eventually become unstable because of the chemistry?

On the practical side, it should be noted that because the gas temperature is (at low density) determined by the molecular abundances, adding chemistry into the stability considerations means that the problem of determining the stability of the MBES becomes also a problem of solving the chemical evolution, with all of the associated complications. As a result, the stability analysis becomes sensitive to a host of new parameters, including for example the initial abundances used for the chemical calculations.

In conclusion, we note that an update of Paper IV, including the effect of chemistry, could yield important new information on the stability of the MBES.

Chapter 8

Summary of the publications

The thesis consists of five journal publications:

- **Paper I: O. Sipilä**, E. Hugo, J. Harju, O. Asvany, M. Juvela, and S. Schlemmer, 2010, "Modelling line emission of deuterated H_3^+ from prestellar cores", Astronomy & Astrophysics, 509, A98

- **Paper II: O. Sipilä**, 2012, "Radial molecular abundances and gas cooling in starless cores", Astronomy & Astrophysics, 543, A38

- **Paper III: O. Sipilä**, P. Caselli, and J. Harju, 2013, "HD depletion in starless cores", Astronomy & Astrophysics, 554, A92

- **Paper IV: O. Sipilä**, J. Harju, and M. Juvela, 2011, "On the stability of non-isothermal Bonnor-Ebert spheres", Astronomy & Astrophysics, 535, A49

- **Paper V:** E. Hardegree-Ullman, J. Harju, M. Juvela, **O. Sipilä**, D.C.B. Whittet, and S. Hotzel, 2013, "Chemical and physical conditions in molecular cloud core DC 000.4–19.5 (SL42) in Corona Australis", The Astrophysical Journal, 763, 45

The papers are summarized below. The author's contribution to the papers is described at the end of each section.

8.1 Paper I

In Paper I, we study the chemistry of prestellar cores in the context of the complete depletion model of Walmsley et al. (2004) and Flower et al. (2004), i.e., assuming that all chemical species containing elements heavier then helium are frozen onto the surfaces of dust grains. Accordingly, the chemical model used in the paper considers mainly gas-phase chemistry, and the only grain-surface reactions are those forming H_2, HD, and D_2. In addition to deuterium, the spin states of the various species are included in the chemical model. We adopt the new state-to-species rate coefficients for the $H_3^+ + H_2$ reacting system published by Hugo et al. (2009). A modified Bonnor-Ebert sphere is used as the physical core model. We divide the model core into concentric spherical shells, and calculate the chemistry separately in each shell. The dust temperature is calculated using a radiative transfer program (we assume $T_{\mathrm{dust}} = T_{\mathrm{gas}}$). We extract steady-state radial abundance profiles from the results of

the chemistry calculations, and use them as input for another radiative transfer program which determines the populations of the various energy levels of the molecules and produces simulated line emission profiles. The simulated line profiles are compared against observations by Harju et al. (2008) toward Oph D and by Vastel et al. (2004) toward I16293E.

We find that the new rate coefficients of Hugo et al. (2009) significantly increase the deuteration degree of H_3^+ compared to the models of Walmsley et al. (2004) and Flower et al. (2004), particularly at low density. We study the density and temperature dependences of the various spin-state ratios and find no uniform behavior between the species studied: for example, the D_3^+ (o/m) ratio is highly density-dependent but changes very little with temperature, while H_2D^+ behaves oppositely. In particular, we find that the H_2D^+ (o/p) ratio increases strongly at low temperature ($< 10\,\text{K}$). We also study the effect of varying the grain radius and the cosmic ray ionization rate on the abundances of the various ions, and also on the spin-state ratios. We find that deuteration is suppressed at large grain radii and at small grain radii, but the spin-state ratios are not in general greatly affected by changes in the grain size, with the exception of the H_2 (o/p) ratio. Increasing the cosmic ray ionization rate decreases deuteration owing to increased electron recombination rates – the situation is reversed for lower cosmic ray ionization rates. Finally, we find that our model gives a reasonably good agreement with the observational results of Harju et al. (2008) and Vastel et al. (2004).

The results indicate that chemical steady-state is reached in a timescale of $\sim 10^5$ years, which is within typical expected core lifetimes. Because the observed H_2D^+ and D_2H^+ column densities are (relatively) high, the model suggests that the observed cores are in an advanced stage of chemical evolution. The new rate coefficients of Hugo et al. (2009) greatly increase deuteration with respect to the models of Walmsley et al. (2004) and Flower et al. (2004) (both studies adopt rate coefficients from the experimental results of Gerlich et al. 2002), indicating that new experiments at low temperature are needed to shed light on the apparent discrepancy between the two measurements.

The author upgraded and performed extensive testing of the gas-phase chemical code initially written by M. Juvela, carried out all of the chemical and radiative transfer calculations, prepared most of the figures and wrote most of the paper. Figures 3, 4 and 9 were contributed by J. Harju. Parts of the text were contributed by Harju and M. Juvela, and the paper was subject to comments and suggestions by the German collaborators.

8.2 Paper II

Paper II studies chemical abundances and the gas temperature in starless cores. For this paper, the chemical model of Paper I was expanded to include gas-grain chemical interaction through adsorption and desorption, and grain surface reactions. Unlike in Paper I, deuterium and spin-state chemistry are not included in the chemical reaction network, but species containing heavy elements (i.e. heavier than helium) in turn are. Initial chemical abundances are calculated based on the dust temperature (the procedure is similar to that of Paper I), and then used as input for radiative transfer calculations that finally determine the gas temperature. The chemical abundances

(and consequently the gas temperature) are studied as functions of core radius and time, and line emission simulations are performed to illustrate the observational effects induced by temporal variation in the chemical abundances. To probe multiple orders of magnitude in density, three different core masses ($0.25\,M_\odot$, $1.0\,M_\odot$ and $5.0\,M_\odot$) are adopted.

We find that the chemical abundances can vary greatly with time owing mainly to molecular depletion. On the other hand, the gas temperature changes only slightly at later stages of core evolution (the typical change in $T_{\rm gas}$ from 10^5 to 10^6 years into the core evolution is only 1-2 K). The cooling of the model cores is mainly controlled by the CO abundance; ^{12}CO is the main coolant molecule even after depletion begins to take effect. However, CO depletion leads to a rise in the gas temperature at late times. Atomic carbon is an important coolant at early times, but its impact decreases dramatically with depletion. Atomic oxygen and O_2 do not contribute appreciably to core cooling. The model predicts that the NH_3/N_2H^+ abundance ratio decreases toward higher densities because of the depletion of ammonia, seemingly contrary to observations. However, this effect occurs only at very high density ($n_{\rm H} > 10^5\,{\rm cm}^{-3}$), and may have been missed by observations; at lower density, our modeling results agree with observations by Tafalla et al. (2002) and Hotzel et al. (2004). Finally, we calculated simulated line emission profiles for ^{13}CO, HCO^+, N_2H^+, and NH_3 and found that the emission profiles vary significantly with time, which implies that core ages may to some extent be constrained based on the strength of the observed emission.

The author expanded the chemical model of Paper I to account for gas-grain chemical interaction by including adsorption and desorption as well as grain-surface chemistry. The author also designed and carried out the calculations yielding simultaneously the various chemical abundance profiles and the gas temperature, prepared all the figures and wrote the paper. The pre-submission draft of the paper was subject to comments by J. Harju.

8.3 Paper III

Paper III expands on the chemical models of Paper I and Paper II by including the deuterated forms of chemical species with up to four atoms and spin-state chemistry for the light species (H_2, H_2^+, and H_3^+) in reactions with species including heavy elements. We compare the new model against the complete depletion model of Walmsley et al. (2004) and Flower et al. (2004), where only the lightest elements (up to He) are included, and thus we do not follow the abundances of, e.g., N_2D^+ and DCO^+ and instead focus on H_2, HD, H_3^+, and its deuterated forms. The adopted physical core model is the $0.25\,M_\odot$ modified Bonnor-Ebert sphere of Paper II, which should be appropriate for comparison against the complete depletion model owing to its very high average density ($n_{\rm H} \sim 8 \times 10^5\,{\rm cm}^{-3}$) and low average temperature (~ 8 K). The chemical abundances and the gas temperature are calculated as in Paper II.

It is usually assumed that the HD abundance stays approximately constant during core evolution, because reactions between H and D on grain surfaces, creating HD, regenerate the gas phase HD abundance as surface HD desorbs. This is also true in the complete depletion model, where heavy elements are assumed to be completely depleted onto grain surfaces and do not contribute to the chemistry (implying that

they are locked in unreactive species, such as water or methanol). The model of Paper III takes into account the heavy element chemistry before depletion occurs, and we find that this leads to eventual HD depletion. The depletion is caused by surface reactions: the deuterated analogues of the $H + O \longrightarrow OH$ and $OH + H \longrightarrow H_2O$ reactions lock deuterium into grain-surface HDO, and consequently HD production through the H+D reaction is diminished. The decrease in the gas phase HD abundance leads to a decrease in deuterium fractionation, and we find that at late times ($\sim 10^6$ years) the deuteration degree of H_3^+ is very low, in stark contrast to the complete depletion model. The spin-state abundance ratios of the various ions are also affected by HD depletion, and generally display strong time-dependence.

The ground-state transitions of $H_2D^+(o)$ and $D_2H^+(p)$ are often quoted as potential probes of the centers of dense cores. Our results indicate that even though HD depletion decreases dramatically the abundances of H_2D^+ and D_2H^+ at very high density, their abundance distibutions eventually become extended because HD is less depleted in the outer, lower-density regions of the core. Thus, HD depletion may influence the interpretation of observations. It should be noted that our results are sensitive to the effects of quantum tunneling (particularly to the tunneling of H_2), and more experimental data on whether tunneling occurs on grain surfaces is urgently needed.

The author designed and wrote the routines that automatically deuterate and spin-state-separate the reactions in the OSU reaction sets. The branching ratios for the various reaction types (listed in Appendix A of the paper) were deduced by the author together with J. Harju. The author carried out all the calculations, prepared all the figures and wrote most of the paper (Sects. 4.2. and 4.6. were contributed by Harju). The paper was subject to comments by P. Caselli and Harju.

8.4 Paper IV

In Paper IV, we study the stability of the modified Bonnor-Ebert sphere (MBES). This study was motivated by Paper I, where we adopted the MBES as the physical core model, but could not quantify whether the model core was stable because the stability condition of the MBES was unknown. To derive the stability condition, we consider equations analogous to those discussed by Bonnor (1956), but assuming instead that $T = T(r)$. This approach leads to a stability condition that is not universal like that of the classical Bonnor-Ebert sphere (BES), but instead depends on how the temperature is determined. We consider two different dust models in the temperature calculations – in the paper, we assume that $T_{\mathrm{dust}} = T_{\mathrm{gas}}$ because we had, at the time, not yet developed the method of self-consistently calculating T_{gas} using chemical abundances (Paper II). The stability is calculated by first fixing the core mass, which yields a series of core configurations with different central densities and temperatures; we then search for the configuration that is critically stable.

We find that the non-dimensional critical radius ξ_1 that characterizes the stability depends on the mass of the core and on the assumed dust model. In general, ξ_1 lies close to ~ 6.5, the critical non-dimensional radius of the BES, but the value increases toward low core masses. The low core mass limit is also the region where the results of the paper are expected to be the most accurate, because low-mass MBESs have very high average densities where the assumption $T_{\mathrm{dust}} = T_{\mathrm{gas}}$ is sound. It is

recognized that the analysis should be repeated with integrated cooling calculations where $T_{\text{dust}} \neq T_{\text{gas}}$ generally (as in Papers II and III) – however, this approach does not remove the ambiguity pertaining to the choice of dust model. In any case, we expect the stability of the MBES to very similar to that of the BES. We also apply the method to studying the stability of very small cores of roughly 10 Jupiter masses to validate or disqualify their possible existence as isolated objects; we find that the external pressure needed to sustain these objects is much higher than that typically found in the ISM.

The author derived the stability condition of the MBES, carried out all the calculations, prepared all the figures presented in the main text and wrote most of the paper. The various mathematical expressions presented in Appendix B were derived by the author together with J. Harju, who also contributed Fig. B.1 and parts of the text in Appendix B. The paper was subject to comments by Harju and M. Juvela.

8.5 Paper V

In Paper V, we study the chemical and physical conditions in SL42, a starless core in Corona Australis. We present $C^{18}O$ and N_2H^+ column density maps based on Swedish ESO Submillimeter Telescope (SEST) observations of the $C^{18}O$ ($J = 2-1, \ 1-0$) and N_2H^+ ($J = 1-0$) transitions. *Herschel* data of the same region is used to map the dust temperature and the H_2 column density. The $C^{18}O$ and N_2H^+ column density profiles as functions of A_V, derived from the column density maps, are compared against predictions from steady-state and time-dependent chemical models.

The column density maps indicate that $C^{18}O$ and N_2H^+ peak at different positions: while the N_2H^+ line is associated with the H_2 column density peak, the $C^{18}O$ profile peaks about $42''$ away from the N_2H^+/H_2 peak. Correlating the $C^{18}O$ column density with visual extinctions derived from Two Micron All Sky Survey (2MASS) and *Herschel* data, we find that the $C^{18}O$ profile indicates depletion toward the core center. The azimuthally averaged H_2 column density profile of the core is well fitted by a Plummer-like density profile, characterized by an r^{-2} dependence away from the core center. Based on an analysis of the total gravitational and kinetic energies of the core, we conclude that the core may be in the early stages of collapse. We combine the (pseudo-time-dependent) chemical model of Paper II with a radiative transfer model and find that the models can reproduce the observed $C^{18}O/N_2H^+$ column density ratio and the observed peak intensities, but the absolute values of the model column densities are clearly lower than the observed ones. Furthermore, the model underestimates the $C^{18}O$ column density for low values of A_V. As an alternative approach, we also attempt to reproduce the observations with a steady-state chemical model and find a reasonably good agreement, although this method does not yield predictions of the N_2H^+ profile and hence it is difficult to conclude whether the steady-state model really is better than the time-dependent model in terms of reproducing the observations.

The author carried out the time-dependent chemical modeling, wrote most of Section 4 and produced Figure 8. The author also contributed to the text in Section 5 and provided general comments on the paper.

Chapter 9

Concluding remarks

In this thesis, we have studied the chemistry and physics of starless and prestellar cores, which were here referred to together as "dense cores". We have concentrated on low-mass cores with high average densities in environments with high external visual extinction, i.e., we have assumed that the cores are embedded in a larger parent cloud – this also means that photoionization for instance is unimportant in our models. Particular attention has been given to the chemistry of H_3^+ and its deuterated counterparts, including their respective spin states (Papers I and III). In addition, more general descriptions of core chemistry (Paper II) and the stability of the cores (Paper IV) have been studied in the thesis. Also, the chemical model has been applied to fitting observed $C^{18}O$ and N_2H^+ abundance profiles (Paper V).

Papers I and III discuss the complete depletion model which was first presented by Walmsley et al. (2004), and has subsequently been widely discussed in the literature. In the complete depletion model, gas-grain chemical interaction is not taken into account except for the formation of H_2 and its deuterated isotopologs on grain surfaces, and this leads to high steady-state abundances of, e.g., H_2D^+ and D_2H^+. In Paper I, we studied how the rate coefficients of the $H_3^+ + H_2$ isotopic system determined recently by Hugo et al. (2009) affect the complete depletion model. In Paper III, we expanded on the complete depletion model by including a full description of gas-grain chemistry which leads to perhaps the main result of this thesis, HD depletion, as deuterium is processed on grain surfaces into heavier deuterium-bearing species such as HDO. HD depletion directly affects the abundances, and possibly the observability, of many tracers of the central areas of dense cores such as H_2D^+ and D_2H^+. In our analysis we imposed a cutoff of four atoms for deuterated species when producing a deuterated version of the OSU reaction network in order to restrict the size of the resultant network and because our analysis concentrates on the lightest species. Realistically, however, deuterium may also be processed into more complex species such as deuterated methanol. For this reason, extension of the deuterium chemistry to species with more than four atoms is needed so that the possible impact on HD depletion, and consequently on the interpretation of observations, can be assessed.

Our results in Papers I and III emphasize the importance of spin-state chemistry to the evolution of deuterium chemistry. Although it has recently received a growing amount of attention in the literature, it can be said that spin-state chemistry should be studied in yet more detail. This point is well illustrated for example by the discussion in Chapter 4 of this thesis and the associated Fig. 4.2, where it is seen that at the low temperatures associated with dense cores, the spin-state abundance ratios are non-

thermal and hence spin-state chemistry will affect the interpretation of observations. In light of our results, it is desirable that models of deuterium and spin-state chemistry are developed in tandem. Of course, experimental data on the reaction rates of various key reactions at low temperature, especially for reactions in which isotopic substitution may play a part, is also sorely needed for the future progress of chemical modeling of dense cores.

The physical properties of dense cores have also been studied in the thesis, albeit only in the particular case of the (modified) Bonnor-Ebert sphere. We have studied core stability in the case of purely thermal support. Even though in Paper II we had to make the simplifying assumption that $T_{\mathrm{dust}} = T_{\mathrm{gas}}$, our results indicate, based on the difference between the two dust models, that even small (1-2 K) changes in temperature may at least moderately influence the stability. Therefore, the stability calculations should be coupled with a chemical model to more accurately model the influence of changes in gas temperature induced by temporal variations in molecular abundances. In the future, the chemical model could be integrated into a (magneto)hydrodynamical core model for a fully self-consistent investigation of the stability.

Although the deuterium chemistry studied in this thesis concentrates on the lightest species such as H_2D^+ and D_2H^+, the chemical model developed during this thesis is, already in its present state, extensive enough to allow for the modeling of the abundances of more massive deuterium-bearing species, such as N_2D^+ and DCO^+. When combined with a radiative transfer model, the chemical model becomes a versatile tool for interpreting observations; a follow-up study of Paper III that includes the modeling of heavier deuterated species and simulated line emission profiles is a logical next step.

The inclusion of the spin states of simple heavy species containing C, N and/or O with multiple protons could be useful not only for constraining observations, but also for improving chemical models. The ortho-to-para ratios of multiple molecules such as water and NH_2D can be observed, and the observed ratios can be used to constrain the models. On the other hand, for some species such as ammonia and H_2D^+ only one of the spin states is observable towards cold cores (from the ground), and thus modeling is needed to understand the total (sum over spin states) abundances of these species. Studies of ammonia and water could be especially important, as the former serves as a thermometer of cold gas (e.g. Juvela et al. 2012) and the latter may be an important coolant at high density (e.g. Goldsmith 2001).

Bibliography

Aikawa, Y., Herbst, E., Roberts, H., & Caselli, P. 2005, The Astrophysical Journal, 620, 330

Aikawa, Y., Ohashi, N., Inutsuka, S.-i., Herbst, E., & Takakuwa, S. 2001, The Astrophysical Journal, 552, 639

Aikawa, Y., Umebayashi, T., Nakano, T., & Miyama, S. M. 1997, The Astrophysical Journal Letters, 486, L51

Aikawa, Y., Wakelam, V., Hersant, F., Garrod, R. T., & Herbst, E. 2012, The Astrophysical Journal, 760, 40

Albertsson, T., Semenov, D. A., Vasyunin, A. I., Henning, T., & Herbst, E. 2013, The Astrophysical Journal Supplement Series, 207, 27

Allen, M. & Robinson, G. W. 1975, The Astrophysical Journal, 195, 81

Allen, M. & Robinson, G. W. 1977, The Astrophysical Journal, 212, 396

Alves, J. F., Lada, C. J., & Lada, E. A. 2001, Nature, 409, 159

Amano, T. & Hirao, T. 2005, J. Mol. Spec., 233, 7

Andersson, S. & van Dishoeck, E. F. 2008, Astronomy & Astrophysics, 491, 907

Bergin, E. A., Alves, J., Huard, T., & Lada, C. J. 2002, The Astrophysical Journal Letters, 570, L101

Bergin, E. A. & Langer, W. D. 1997, The Astrophysical Journal, 486, 316

Bergin, E. A., Maret, S., van der Tak, F. F. S., et al. 2006, The Astrophysical Journal, 645, 369

Biham, O., Furman, I., Pirronello, V., & Vidali, G. 2001, The Astrophysical Journal, 553, 595

Bonnor, W. B. 1956, Monthly Notices of the Royal Astronomical Society, 116, 351

Bourke, T. L., Hyland, A. R., Robinson, G., James, S. D., & Wright, C. M. 1995, Monthly Notices of the Royal Astronomical Society, 276, 1067

Cardelli, J. A., Mathis, J. S., Ebbets, D. C., & Savage, B. D. 1993, The Astrophysical Journal Letters, 402, L17

Caselli, P., Hasegawa, T. I., & Herbst, E. 1998, The Astrophysical Journal, 495, 309

Caselli, P., Keto, E., Bergin, E. A., et al. 2012, The Astrophysical Journal Letters, 759, L37

Caselli, P., van der Tak, F. F. S., Ceccarelli, C., & Bacmann, A. 2003, Astronomy & Astrophysics, 403, L37

Caselli, P., Vastel, C., Ceccarelli, C., et al. 2008, Astronomy & Astrophysics, 492, 703

Caselli, P., Walmsley, C. M., Zucconi, A., et al. 2002, The Astrophysical Journal, 565, 344

Cazaux, S., Caselli, P., Cobut, V., & Le Bourlot, J. 2008, Astronomy & Astrophysics, 483, 495

Cazaux, S., Caselli, P., & Spaans, M. 2011, The Astrophysical Journal Letters, 741, L34

Cazaux, S., Cobut, V., Marseille, M., Spaans, M., & Caselli, P. 2010, Astronomy & Astrophysics, 522, A74

Cazaux, S. & Spaans, M. 2009, Astronomy & Astrophysics, 496, 365

Cazaux, S. & Tielens, A. G. G. M. 2004, The Astrophysical Journal, 604, 222

Charnley, S. B., Tielens, A. G. G. M., & Rodgers, S. D. 1997, The Astrophysical Journal Letters, 482, L203

Cuppen, H. M. & Herbst, E. 2007, The Astrophysical Journal, 668, 294

Cuppen, H. M., van Dishoeck, E. F., Herbst, E., & Tielens, A. G. G. M. 2009, Astronomy & Astrophysics, 508, 275

de Geus, E. J., de Zeeuw, P. T., & Lub, J. 1989, Astronomy & Astrophysics, 216, 44

d'Hendecourt, L. B., Leger, A., Olofsson, G., & Schmidt, W. 1986, Astronomy & Astrophysics, 170, 91

di Francesco, J., Evans, II, N. J., Caselli, P., et al. 2007, Protostars and Planets V, 17

Dickens, J. E., Irvine, W. M., Snell, R. L., et al. 2000, The Astrophysical Journal, 542, 870

Doty, S. D., Everett, S. E., Shirley, Y. L., Evans, N. J., & Palotti, M. L. 2005, Monthly Notices of the Royal Astronomical Society, 359, 228

Draine, B. T. & Li, A. 2001, The Astrophysical Journal, 551, 807

Draine, B. T. & Sutin, B. 1987, The Astrophysical Journal, 320, 803

Du, F. & Parise, B. 2011, Astronomy & Astrophysics, 530, A131

Duley, W. W. 1985, The Astrophysical Journal, 297, 296

Duley, W. W. & Williams, D. A. 1984, Interstellar Chemistry (Academic Press)

Dyson, J. & Williams, D. 1997, The Physics of the Interstellar Medium, Second Edition (IOP Publising Ltd)

Ebert, R. 1955, Zeitschrift für Astrophysik, 37, 217

Evans, II, N. J., Rawlings, J. M. C., Shirley, Y. L., & Mundy, L. G. 2001, The Astrophysical Journal, 557, 193

Flower, D. R. & Pineau des Forêts, G. 2003, Monthly Notices of the Royal Astronomical Society, 343, 390

Flower, D. R., Pineau des Forêts, G., & Walmsley, C. M. 2004, Astronomy & Astrophysics, 427, 887

Flower, D. R., Pineau Des Forêts, G., & Walmsley, C. M. 2005, Astronomy & Astrophysics, 436, 933

Flower, D. R., Pineau Des Forêts, G., & Walmsley, C. M. 2006a, Astronomy & Astrophysics, 456, 215

Flower, D. R., Pineau Des Forêts, G., & Walmsley, C. M. 2006b, Astronomy & Astrophysics, 449, 621

Fontani, F., Caselli, P., Zhang, Q., et al. 2012, Astronomy & Astrophysics, 541, A32

Galli, D., Walmsley, M., & Gonçalves, J. 2002, Astronomy & Astrophysics, 394, 275

Garrod, R. T. 2008, Astronomy & Astrophysics, 491, 239

Garrod, R. T. & Herbst, E. 2006, Astronomy & Astrophysics, 457, 927

Garrod, R. T. & Pauly, T. 2011, The Astrophysical Journal, 735, 15

Garrod, R. T., Wakelam, V., & Herbst, E. 2007, Astronomy & Astrophysics, 467, 1103

Gerlich, D., Herbst, E., & Roueff, E. 2002, Planet. Space Sci., 50, 1275

Goldsmith, P. F. 2001, The Astrophysical Journal, 557, 736

Goldsmith, P. F. & Langer, W. D. 1978, The Astrophysical Journal, 222, 881

Gould, R. J. & Salpeter, E. E. 1963, The Astrophysical Journal, 138, 393

Goumans, T. P. M. & Andersson, S. 2010, Monthly Notices of the Royal Astronomical Society, 406, 2213

Gredel, R., Lepp, S., Dalgarno, A., & Herbst, E. 1989, The Astrophysical Journal, 347, 289

Harju, J., Juvela, M., Schlemmer, S., et al. 2008, Astronomy & Astrophysics, 482, 535

Hartmann, L., Ballesteros-Paredes, J., & Bergin, E. A. 2001, The Astrophysical Journal, 562, 852

Hasegawa, T. I. & Herbst, E. 1993a, Monthly Notices of the Royal Astronomical Society, 261, 83

Hasegawa, T. I. & Herbst, E. 1993b, Monthly Notices of the Royal Astronomical Society, 263, 589

Hasegawa, T. I., Herbst, E., & Leung, C. M. 1992, The Astrophysical Journal Supplement Series, 82, 167

Herbst, E. & Klemperer, W. 1973, The Astrophysical Journal, 185, 505

Herbst, E. & van Dishoeck, E. F. 2009, Annual Review of Astronomy & Astrophysics, 47, 427

Hinshelwood, C. N. 1940, The Kinetics of Chemical Change (The Clarendon Press)

Ho, P. T. P. & Townes, C. H. 1983, Annual Review of Astronomy & Astrophysics, 21, 239

Hollenbach, D. & Salpeter, E. E. 1971, The Astrophysical Journal, 163, 155

Hotzel, S., Harju, J., & Walmsley, C. M. 2004, Astronomy & Astrophysics, 415, 1065

Hugo, E., Asvany, O., & Schlemmer, S. 2009, J. Chem. Phys., 130, 164302

Juvela, M. 1997, Astronomy & Astrophysics, 322, 943

Juvela, M., Harju, J., Ysard, N., & Lunttila, T. 2012, Astronomy & Astrophysics, 538, A133

Juvela, M. & Ysard, N. 2011, The Astrophysical Journal, 739, 63

Katz, N., Furman, I., Biham, O., Pirronello, V., & Vidali, G. 1999, The Astrophysical Journal, 522, 305

Keto, E. & Caselli, P. 2008, The Astrophysical Journal, 683, 238

Keto, E. & Caselli, P. 2010, Monthly Notices of the Royal Astronomical Society, 402, 1625

Keto, E. & Field, G. 2005, The Astrophysical Journal, 635, 1151

Kirk, H., Johnstone, D., & Tafalla, M. 2007, The Astrophysical Journal, 668, 1042

Langmuir, I. 1922, Transactions of the Faraday Society, 17, 621

Le Bourlot, J. 1991, Astronomy & Astrophysics, 242, 235

Le Petit, F., Barzel, B., Biham, O., Roueff, E., & Le Bourlot, J. 2009, Astronomy & Astrophysics, 505, 1153

Léger, A., Jura, M., & Omont, A. 1985, Astronomy & Astrophysics, 144, 147

Li, A. & Draine, B. T. 2002, The Astrophysical Journal, 564, 803

Linsky, J. L. 2003, Space Science Reviews, 106, 49

Maret, S., Bergin, E. A., & Lada, C. J. 2007, The Astrophysical Journal Letters, 670, L25

McKee, C. F. 1989, The Astrophysical Journal, 345, 782

Mestel, L. & Spitzer, Jr., L. 1956, Monthly Notices of the Royal Astronomical Society, 116, 503

Meyer, D. M., Jura, M., & Cardelli, J. A. 1998, The Astrophysical Journal, 493, 222

Mouschovias, T. C., Tassis, K., & Kunz, M. W. 2006, The Astrophysical Journal, 646, 1043

Myers, P. C. & Benson, P. J. 1983, The Astrophysical Journal, 266, 309

Neufeld, D. A., Lepp, S., & Melnick, G. J. 1995, The Astrophysical Journal Supplement Series, 100, 132

Nielbock, M., Launhardt, R., Steinacker, J., et al. 2012, Astronomy & Astrophysics, 547, A11

Oka, T. 2004, J. Mol. Spectrosc., 228, 635

Oppenheimer, M. & Dalgarno, A. 1974, The Astrophysical Journal, 192, 29

Pagani, L., Bacmann, A., Cabrit, S., & Vastel, C. 2007, Astronomy & Astrophysics, 467, 179

Pagani, L., Salez, M., & Wannier, P. G. 1992, Astronomy & Astrophysics, 258, 479

Pagani, L., Vastel, C., Hugo, E., et al. 2009, Astronomy & Astrophysics, 494, 623

Parise, B., Belloche, A., Du, F., Güsten, R., & Menten, K. M. 2011, Astronomy & Astrophysics, 526, A31

Park, I. H., Wakelam, V., & Herbst, E. 2006, Astronomy & Astrophysics, 449, 631

Perets, H. B. & Biham, O. 2006, Monthly Notices of the Royal Astronomical Society, 365, 801

Prasad, S. S. & Tarafdar, S. P. 1983, The Astrophysical Journal, 267, 603

Roberts, J. F., Rawlings, J. M. C., Viti, S., & Williams, D. A. 2007, Monthly Notices of the Royal Astronomical Society, 382, 733

Rodgers, S. D. & Millar, T. J. 1996, Monthly Notices of the Royal Astronomical Society, 280, 1046

Ruffle, D. P. & Herbst, E. 2000, Monthly Notices of the Royal Astronomical Society, 319, 837

Semenov, D., Hersant, F., Wakelam, V., et al. 2010, Astronomy & Astrophysics, 522, A42

Stahler, S. W. & Yen, J. J. 2010, Monthly Notices of the Royal Astronomical Society, 407, 2434

Stark, R., van der Tak, F. F. S., & van Dishoeck, E. F. 1999, The Astrophysical Journal Letters, 521, L67

Tafalla, M., Myers, P. C., Caselli, P., Walmsley, C. M., & Comito, C. 2002, The Astrophysical Journal, 569, 815

Tafalla, M., Santiago-García, J., Myers, P. C., et al. 2006, Astronomy & Astrophysics, 455, 577

Taquet, V., Ceccarelli, C., & Kahane, C. 2012, Astronomy & Astrophysics, 538, A42

Taquet, V., Peters, P. S., Kahane, C., et al. 2013, Astronomy & Astrophysics, 550, A127

Tielens, A. G. G. M. 1983, Astronomy & Astrophysics, 119, 177

Tielens, A. G. G. M. & Hagen, W. 1982, Astronomy & Astrophysics, 114, 245

van Dishoeck, E. F. & Blake, G. A. 1998, Annual Review of Astronomy & Astrophysics, 36, 317

Vastel, C., Caselli, P., Ceccarelli, C., et al. 2006, The Astrophysical Journal, 645, 1198

Vastel, C., Phillips, T. G., & Yoshida, H. 2004, The Astrophysical Journal Letters, 606, L127

Vasyunin, A. I., Semenov, D. A., Wiebe, D. S., & Henning, T. 2009, The Astrophysical Journal, 691, 1459

Wakelam, V. & Herbst, E. 2008, The Astrophysical Journal, 680, 371

Walmsley, C. M., Flower, D. R., & Pineau des Forêts, G. 2004, Astronomy & Astrophysics, 418, 1035

Watanabe, N., Kimura, Y., Kouchi, A., et al. 2010, The Astrophysical Journal Letters, 714, L233

Williams, D. & Herbst, E. 2002, Surface Science, 500, 823

Witt, A. N. & Schild, R. E. 1988, The Astrophysical Journal, 325, 837

Woodall, J., Agúndez, M., Markwick-Kemper, A. J., & Millar, T. J. 2007, Astronomy & Astrophysics, 466, 1197